Calcium signaling through a Transient Receptor Channel is important for *Toxoplasma gondii* growth

Karla M. Márquez-Nogueras[1,2], Nathan M. Chasen[1], Myriam A. Hortua Triana[1], Ivana Y. Kuo[2], Silvia N.J. Moreno[1]

[1]Center for Tropical and Emerging Global Diseases, Department of Computes Science, University of Georgia and [3]Department of Cellular Biology, University of Georgia, Athens, Georgia 30602
Department of Cell and Molecular Physiology, Stritch School of Medicine, Loyola University Chicago, Maywood IL, 60132

Running title: TRPPL-2 mediates calcium influx in *T. gondii*

*To whom correspondence should be addressed: Silvia N. J. Moreno, Department of Cellular Biology and Center for Tropical and Emerging Global Disease, 350A Paul D. Coverdell Center, University of Georgia, Athens, GA 30602. Tel.: 706-542-4736; Fax: 706-542-9493; E-mail: smoreno@uga.edu

Keywords: Calcium TRP Channel, Signaling, *Toxoplasma gondii*

ABSTRACT

Transient Receptor Potential (TRP) channels participate in calcium (Ca^{2+}) influx and intracellular Ca^{2+} release. TRP channels have not been studied in *Toxoplasma gondii* or any other Apicomplexan parasite. We characterized TgGT1_310560, a gene predicted to possess a TRP domain (TgTRPPL-2) and determined its role in Ca^{2+} signaling in *T. gondii*, the causative agent of toxoplasmosis. TgTRPPL-2 localized to the plasma membrane and the endoplasmic reticulum of *T. gondii*. *ΔTgTRPPL-2* mutants were defective in growth and Ca^{2+} influx. Heterologous expression of TgTRPPL-2 in HEK-3KO cells allowed its functional characterization. Patching of ER-nuclear membranes demonstrated that TgTRPPL-2 is a non-selective cation channel that conducts Ca^{2+}. Pharmacological blockers of TgTRPPL-2 inhibited Ca^{2+} influx and parasite growth. This is the first report of an Apicomplexan channel that conducts Ca^{2+} and initiates the Ca^{2+} signaling cascade that culminates in the stimulation of motility, invasion and egress. TgTRPPL-2 is a potential target for combating Toxoplasmosis.

INTRODUCTION

Ca^{2+} signaling is universal and forms part of the signaling pathways that activate or modulate a variety of physiological responses like gene transcription, muscle contraction, cell differentiation and proliferation [1]. Ca^{2+} signals can be generated through the opening of ion channels that allow the downward flow of Ca^{2+} from either outside the cell or from intracellular stores like the endoplasmic reticulum [2].

Toxoplasma gondii is an intracellular parasite from the Apicomplexan phylum, that causes toxoplasmosis in humans [3]. Infection with *T. gondii* may lead to severe complications in immunocompromised patients like encephalitis, myocarditis and death [4]. The *T. gondii* tachyzoite engages in a lytic cycle directly responsible for the pathogenicity of the infection as it results in lysis of host cells [5]. The lytic cycle consists of active invasion of host cells, replication inside a parasitophorous vacuole and egress to search for a new host cell to invade. Ca^{2+} signals resulting from Ca^{2+} influx or from intracellular release, trigger a signaling cascade in the parasite that culminates in the stimulation of essential features of its lytic cycle, like motility, invasion, egress and secretion of proteins essential for attachment to the host cell [6, 7].

Previous work from our lab showed the presence of a Ca^{2+} influx activity at the plasma membrane of *T. gondii* tachyzoites that was functional in extracellular tachyzoites [8] and intracellular replicating parasites [9]. The application of voltage operated Ca^{2+} channel blockers such as nifedipine inhibited ~ 80% of Ca^{2+} influx, and the residual Ca^{2+} entry activity suggested the potential existence of more than one channel at the plasma membrane of *T. gondii* [8]. The molecular entity of these channels has remained elusive.

Transient Receptor Potential (TRP) channels are a large family of cation permeable channels grouped into seven subfamilies based on their gene sequence [10]. TRP channels can be activated by a multitude of stimuli and are involved in a wide range of cellular functions [11]. Most TRP channels are permeable to Ca^{2+} and all of them are permeable to monovalent cations [11]. Some

TRP channels can participate in Ca^{2+} influx as well as Ca^{2+} release from intracellular stores [12, 13]. Mutations in these molecules are associated with a diverse set of diseases, due to their wide distribution in various tissues and their roles in pathological conditions like cancer and renal physiology making these channels important therapeutic targets [14]. The polycystin TRP (TRPP) subfamily of proteins are implicated in Autosomal Dominant Polycystic Kidney Disease (ADPKD) [15].

Predicted protein sequences with TRP domains have been found in most parasitic protozoa, although in lower numbers and types than in other organisms [16]. This could be the result of the evolutionary distance between the species studied, or because of loss of specific functions resulting from evolution of the parasitic lifestyle [16]. A genome analysis of a number of pathogenic protozoan parasites [17] searching for genes with homology to mammalian Ca^{2+} channels identified two *T. gondii* hypothetical genes (TgGT1_247370 and TgGT1_310560) with homologous regions to the TRPP family [18]. We termed these genes *TgTRPPL-1* and *TgTRPPL-2*. Previous work from our laboratory, localized TgTRPPL-1 to the ER with high resolution tags due to its low level of expression [19].

In this work we characterize TgTRPPL-2 in *T. gondii*, which represents the first TRP cation channel studied in any Apicomplexan parasite. Using reverse genetic approaches, we determine the role of TgTRPPL-2 in the lytic cycle of the parasite. We also characterize the electrophysiological features of TgTRPPL-2 and its role in Ca^{2+} influx and, interestingly, find that pharmacological agents that block the activity of TgTRPPL-2 also inhibited Ca^{2+} influx in the parasite and parasite growth. TgTRPPL-2 emerges as one of the molecular entities involved in initiating Ca^{2+} signals in *T. gondii*.

RESULTS

TgTRPPL-2 (TgGT1_310560) localizes to the plasma membrane and the endoplasmic reticulum

Two genes in the *T. gondii's* genome annotated as hypothetical proteins possess Polycystic Kidney Disease (PKD) domains, which are characteristic of the Subfamily P (polycystin) of TRP channels. Mammalian TRPP channels contain 6 transmembrane domains with a large extracellular loop between the first and second transmembrane domain [20]. We termed these molecules in *T. gondii* TgTRPPL-1 (TgGT1_247370) and TgTRPPL-2 (TgGT1_310560). Using BLAST to compare the amino acid sequences of the mammalian *PKD2* and *TgTRPPL-2* showed low sequence homology (21.7%), even at the PKD Domains. The *TgGT1_310560* gene predicts the expression of a protein of 2,191 amino acids with an apparent molecular weight of 237 kDa and 14 transmembrane domains. The predicted topology [21] showed a large extracellular loop between the first and second transmembrane domain, which is characteristic of PKD Channels (Fig. 1A, *TgGT1_310560 cartoon*). Because our initial analysis showed low sequence homology, we next analyzed the amino acid sequence using the software HHPred, which searches for homology based on protein sequence and secondary structure [22]. Sequence analysis of TgTRPPL-2 showed high homology to mammalian PKD2, and the top 10 hits are homologous to PKD2 of a variety of organisms (Table S1).

To investigate the localization of TgTRPPL-2, we introduced the high affinity tag smHA [19] at the 3' terminus of the *TgTRPPL-2* locus and isolated TgTRPPL-2-smHA cell clones. Carboxy-terminus tagging was done in the parental line RHTatiΔku80 (*TatiΔku80*) which favors homologous recombination [23]. Correct incorporation of the tag in the TgTRPPL-2-smHA line was validated by PCR (Fig. S1A) and western blot analysis using anti-HA antibodies (Fig. 1B). A band of approximately ~150 kDa was observed in lysates of TgTRPPL-2-smHA tachyzoites, which is nearly 87 kDa smaller (Fig. 1B) than the predicted size of 237 kDa without taking into account the smHA tag (~39 kDa).

Interestingly, a recent release of ToxoDBv.45 presents additional models for the *TgGT1_310560* gene from different *T. gondii* strains. The gene model for *TgVAND_310560* shows two fragments, *TgVAND_310560A,* which predicts a protein with 9 TMD and a size of ~107.97 kDa and *TgVAND_310560B*, which predicts a protein with 6 TMD and a size of ~116.6 kDa. Sequence alignments of the *TgGT1_310560* gene with the gene models for the VAND strain (A and B) shows 98% homology between them (Fig. 1C). The *T. gondii* VAND strain is an isolate from South America and belongs to the hypervirulent Type I group, as the GT1 and RH strains. According to the gene model of the VAND strain, the predicted MW of the TgVAND_310560B protein would be similar to the band size observed in our western blots (116.6 + 39) with a predicted topology of 6 TMD, in closer agreement with typical TRP channels [24, 25].

To further demonstrate that the protein band observed in the western blot analysis corresponded to the tagged TgTRPPL-2 gene, we performed immunoprecipitations with anti-HA of lysates from the TgTRPPL-2-smHA cells. The immunoprecipitated samples were developed in a PAGE gel. The ~150 kDa band was sliced and analyzed by mass spectrometry (Fig. S1B, *red box*)(Table S2). According to the results, approximately ~700 amino acids toward the C-terminus domain were covered by the peptides corresponding to a 66% coverage. Comparison of the coverage with the TgVAND_310560B predicted protein, approximately 66% of the sequence was recovered by the mass spectrometry analysis. This result indicated that the TgGT1_310560 is likely cleaved, a characteristic common with other TRP channels [26].

We next investigated the cellular location of TgTRPPL-2. Immunofluorescence analysis (IFAs) of extracellular and intracellular parasites showed that TgTRPPL-2-smHA may localize to peripheral vesicles close to the plasma membrane and to the endoplasmic reticulum (ER) (Fig. 1D-E). Some co-localization with the plasma membrane surface antigen (Sag1) and the sarco-endoplasmic reticulum Ca^{2+} ATPase (TgSERCA) (ER marker) was observed (Fig. 1D-E). However, considering the low-level of expression of TgTRPPL-2, it was difficult to draw definitive conclusions about its localization.

We next raised polyclonal antibodies against a fragment peptide of TgTRPPL-2, which is indicated in Fig. 1A (*highlighted in green*). The peptide was expressed in bacteria, purified and used for immunization of mice. Mouse serum was isolated and affinity purified prior to its use for IFAs. The localization at the periphery of extracellular tachyzoites was further confirmed by co-localization with αSAG1 (Fig. 1F). In addition, extracellular tachyzoites showed intracellular staining that co-localized with TgSERCA (Fig. 1F) supporting ER localization. Additionally, IFAs

of intracellular tachyzoites showed that TgTRPPL-2 co-localized with αSAG1 and αSERCA (Fig.1G).

In summary, TgTRPPL-2 is expressed in *T. gondii* tachyzoites, it is likely post-translationally cleaved and localizes to the PM and the ER.

TgTRPPL-2 is important for growth, invasion and egress of Toxoplasma gondii

With the aim to investigate the physiological role of TgTRPPL-2 in *T. gondii,* we generated *ΔTgTRPPL-2* mutants using the CRISPR-Cas9 approach to disrupt the transcription of *TgTRPPL-2* by inserting a dihydrofolate reductase-thymidylate synthase (DHFR) cassette in the *TgTRPPL-2* genomic locus (Fig. 2A). Genetic controls for the insertion were done by PCR, and qPCR showed a significant decrease in the levels of *TgTRPPL-2* transcripts (Fig. 2B).

We next complemented the *ΔTgTRPPL-2* mutants with Cosmid PSBLZ13 [27] that contains the whole genomic locus of the *TgTRPPL-2* gene and generated the cell line *ΔTgTRPPL-2-trppl2*. Controls for the expression of *TgTRPPL-2* was done by qPCR and by IFAs, which further confirmed the identity of the tagged gene, as it was not expressed in the *ΔTgTRPPL-2* mutants and was present in the complemented line *ΔTgTRPPL-2-trppl2* (Fig. 2B-C). Further validation of the absence of expression of TgTRPP2-L and its complementation is shown in Figs S2A-B with additional IFA images and westerns of the *ΔTgTRPPL-2* and *ΔTgTRPPL-2-trppl2* (Fig S2B).

We next evaluated if the expression of *TgTRPPL-2* would impact *T. gondii* growth by plaque assays, in which the parasite engages in repetitive cycles of invasion, replication, and egress causing host cell lysis and formation of plaques observed as white spots by staining with crystal violet. The *ΔTgTRPPL-2* parasites formed smaller plaques compared to its parental counterpart indicating a growth defect (Fig. 2D). This growth defect was partially restored in the complemented cell line (Fig. 2D). We reasoned that the overexpression of *TgTRPPL-2* in the *ΔTgTRPPL-2-trppl2* mutants likely affect parasite fitness masking the rescue effect.

To determine which step of the lytic cycle was affected we performed invasion and egress assays. For invasion we used the red green assay [28] under two extracellular Ca^{2+} (1.8 and 0.5 mM) conditions. Quantification of invasion in the presence of 1.8 mM Ca^{2+} showed a lower invasion rate for the *ΔTgTRPPL-2* (Fig. 2E). Reducing the extracellular concentration of Ca^{2+} to 0.5 mM resulted in a reduced rate of invasion by the parental cells, which was similar to the invasion rate of the *ΔTgTRPPL-2* mutants. This result demonstrated that TgTRPPL-2 is important for invasion at higher concentrations of extracellular Ca^{2+}.

Egress of intracellular tachyzoites can be triggered by permeabilizing infected host cells with saponin in the presence of a buffer containing 1.8 mM of extracellular Ca^{2+}. Under these conditions egress of the *ΔTgTRPPL-2* mutants was slower than egress of the parental strain (Fig. 2F). Additionally, when egress was stimulated by Zaprinast, which increases cytosolic Ca^{2+}, also resulted in the *ΔTgTRPPL-2* mutants taking longer to egress (Fig. 2G). For both assays tested, the *ΔTgTRPPL-2* mutants took twice the time to egress compared to the parental line.

In summary, disruption of the TgTRPPL-*2* locus negatively impacted two important steps of the *T. gondii* lytic cycle, invasion and egress, which impacted parasite growth.

The role TgTRPPL-2 in Ca^{2+} influx

We previously showed that *T. gondii* tachyzoites allow influx of Ca^{2+} when exposed to 2 mM extracellular Ca^{2+} [8]. To determine the role of TgTRPPL-2 in this pathway, we loaded *ΔTgTRPPL-2* parasites with Fura-2AM to study intracellular Ca^{2+} changes after exposing them to 1.8 mM extracellular Ca^{2+} (Fig. 3A). The resting cytosolic Ca^{2+} concentration of *ΔTgTRPPL-2* mutants was around 75 nM which is similar to the resting concentration of parental cells (~70-100 nM). Adding 1.8 mM to the extracellular buffer caused an increase in cytosolic Ca^{2+} in both the parental strain and the *ΔTgTRPPL-2* mutants (Fig. 3B). However, Ca^{2+} influx of the *ΔTgTRPPL-2* mutants was significantly lower (Fig. 3C) and it was decreased almost 50%. The *ΔTgTRPPL-2-trppl2* complemented mutants, however, regained the Ca^{2+} influx activity and they even showed higher Ca^{2+} influx than parental cells, consistent with the higher expression of *TgTRPPL-2* shown by qPCR (Fig. 2B). The reduction of Ca^{2+} influx was further confirmed when adding 1 mM extracellular calcium to the *ΔTgTRPPL-2* mutants (Fig. S3A).

When *T. gondii* tachyzoites are suspended in a high Ca^{2+} buffer from the beginning of the experiment there is a slow constitutive influx of Ca^{2+}, that we attribute to leakage through a PM channel (Fig. 3D, *parental black tracing*). Interestingly, this leakage activity was significantly reduced in the *ΔTgTRPPL-2* mutants (Fig. 3D-E, *blue tracing and bar*), supporting a role of TgTRPPL-2 in constitutive Ca^{2+} influx at the PM. Additional evidence is provided by the enhanced Ca^{2+} leakage observed with the *ΔTgTRPPL-2-trppl2* complemented mutants (Fig. 3D-E, *purple tracing and bar*). The high Ca^{2+} leakage and Ca^{2+} influx observed with the *ΔTgTRPPL-2-trppl2* mutants may affect parasite fitness and would explain the partial growth recovery of these mutants.

Ca^{2+} channels may also be modulated by Ca^{2+} itself [29]. We previously showed that a cytosolic $[Ca^{2+}]$ increase may activate Ca^{2+} influx at the PM (Ca^{2+} activated Ca^{2+} entry) [8]. We next investigated if the Ca^{2+} activated Ca^{2+} entry (CACE) activity was due to the functioning of TgTRPPL-2 at the PM. We added thapsigargin (Thap) to tachyzoites in suspension (Fig. 3F), which results in a cytosolic Ca^{2+} increase due to inhibition of the SERCA-Ca^{2+}-ATPase (SERCA) resulting in uncompensated Ca^{2+} efflux into the cytosol. This elevated cytosolic Ca^{2+} stimulates further Ca^{2+} influx at the PM, which we assessed as an increase in cytosolic Ca^{2+} following addition of high Ca^{2+} to the buffer (Fig 3F, *black tracing*). Note that the $\Delta[Ca^{2+}]_{cyt}$ shown in Fig. 3H, *black column*, is almost 2.5 times higher than the $\Delta[Ca^{2+}]_{cyt}$ observed without previous addition of thap (Fig. 3C, *black column*). This CACE activity was absent in the *ΔTgTRPPL-2* mutants (Fig. 3F, *blue tracing*) but was restored in the *ΔTgTRPPL-2-trppl2* complemented strain (Fig. 3F, *purple tracing*). Quantifications of the rate of Ca^{2+} increase after adding Ca^{2+} and statistical analyses are shown in Fig. 3G-H. Note that the *ΔTgTRPPL-2* mutants showed a reduced response to the addition of thap and also to the addition of Ca^{2+}. Comparing the response to the addition of extracellular Ca^{2+} shown in Fig. 3H, *blue column*, the $\Delta[Ca^{2+}]_{cyt}$ is similar to the one measured

directly without previous addition of Thap (compare with the *blue column* in Fig 3C). This result points to a complete absence of the modulatory effect of cytosolic Ca^{2+} on the PM Ca^{2+} influx in the *ΔTgTRPPL-2* mutants which is restored in the *ΔTgTRPPL-2-trppl2* parasites.

We next tested Zaprinast, which increases the levels of cGMP resulting in Ca^{2+} release from an unidentified store [30]. We previously showed the Ca^{2+} release was almost 2.5 times higher in the presence of extracellular Ca^{2+} compared with the absence of extracellular Ca^{2+} [30]. We attributed this increase to stimulation of the PM Ca^{2+} channel by cytosolic Ca^{2+} (CACE). When testing this phenotype with the *ΔTgTRPPL-2* mutants, we observed that the increased response was absent (Fig. 3I-K). Also note that even the release of Ca^{2+} from intracellular stores by Zaprinast in the presence of low extracellular Ca^{2+} (~50 nM) was significantly decreased in the *ΔTgTRPPL-2* mutants (Fig. S3B-C). The modulatory action of elevated cytosolic Ca^{2+} in Ca^{2} influx was absent in the *ΔTgTRPPL-2* mutants (Fig. 3I-K).

Taken together, these results support a role for TgTRPPL-2 in Ca^{2+} influx at the PM. In addition, TgTRPPL-2 is modulated by cytosolic Ca^{2+} and it is responsible for a constitutive PM Ca^{2+} influx pathway.

TgTRPPL-2 is a cation conducting channel

With the aim of establishing whether TgTRPPL-2 functions as a channel and if it is able to conduct Ca^{2+} we cloned the cDNA of the *TgTRPPL-2* gene into a mammalian expression vector (pCDNA3.1) for expression in human embryonic kidney 293 cells (HEK-3KO) [31]. These HEK cell line is genetically modified and the 3 isoforms of the inositol 1,4,5-trisphosphate receptor (IP_3R) are deleted, to reduce background Ca^{2+} currents [31]. TgTRPPL-2 was mostly expressed at the ER of HEK cells as assessed by co-localization with a red fluorescent protein (RFP) targeted to the ER and compared with the mammalian homolog Polycystin 2 (PC2) (Fig. 4A). Because of this, we isolated nuclear/ER membranes (Fig. 4B) for single channel patch clamp experiments and further characterization of the permeability properties of TgTRPPL-2 (Fig. 4C).

In the presence of 1.8 mM of Ca^{2+} inside the patch pipette and 100 nM of Ca^{2+} in the bath solution (see scheme of Fig. 4B), the membranes isolated from control cells, held at –80 mV, showed very little activity and the conductance remained at less than 1.5 pA (Fig. 4D, *control tracing*). Some channel activity was observed after artificially depolarizing membranes (–80 to +20 mV) presumably due to opening of potassium channels. In comparison, when analyzing membranes isolated from cells expressing TgTRPPL-2 a significant increase in the open probability and current sizes was observed (Fig. 4D, *TgTRPPL-2 blue tracing*). The current-voltage relationship was linear and significantly different from the one from control cells (Fig. 4E, *blue vs. black line*).

We compared the activity of TgTRPPL-2 with the mammalian PKD Channel PC2 in parallel experiments since PC2 has been well characterized in the literature. Activity of PC2 expressing cells displayed a voltage-dependent behavior, as the current-voltage relationship was not linear, with a conductance of ~73 pS (Fig. 4D-E, *red tracing*). Previous work has demonstrated that PC2 can be voltage dependent. Additionally, depending on the experimental setup, conductance for

PC2 can be variable. Comparing our experimental approach to previous work, conductance for PC2 in a high Ca^{2+} solution is similar (~73 pS vs. ~ 97 pS). Although TgTRPPL-2 does not appear to be voltage dependent, conductance of the channel is similar to its mammalian homologue.

Ca^{2+} is able to modulate the activity of channels and TRP-P channels have been shown to be activated by Ca^{2+} as some of them have an EF-hand motif at the C-terminus [29, 32]. To determine whether Ca^{2+} is able to modulate the activity of TgTRPPL-2 we first varied the [Ca^{2+}] inside the pipette (in equilibrium with the ER lumen). When the Ca^{2+} concentration was increased to 10 mM Ca^{2+} there was a significant inhibition of TgTRPPL-2 channel activity. With high Ca^{2+} concentration, the channel displayed voltage-dependent inhibition over the -75 to -25 mV range and conductance was significantly decreased (Fig. 4F). In the presence of 1.8 mM Ca^{2+} inside the pipette, TgTRPPL-2 had a conductance of ~55 pS, which is significantly higher than the conductance calculated for control membranes. The conductance decreased to ~21 pS when Ca^{2+} was increased to 10 mM.

Although no evidence for a conserved EF-hand motif was found in TgTRPPL-2 we checked for the potential modulation by cytosolic Ca^{2+}. Increasing the concentration of Ca^{2+} in the bath solution from 100 nM to 10 μM (which would simulate changes in cytosolic Ca^{2+}), enhanced channel activity from membranes expressing TgTRPPL-2 (Fig. 4G-H, *blue vs. gold line*). Interestingly, increasing the [Ca^{2+}] only increased the open probability when the membrane was depolarized to -80 mV (Fig. 4I). However, increase of the [Ca^{2+}] of the bath solution, increased the conductance of the channel almost 2.5x, suggesting modulation of the channel by Ca^{2+} itself. In conclusion, these data indicate that TgTRPPL-2 is able to conduct Ca^{2+} currents and is modulated by cytosolic Ca^{2+}.

To distinguish whether TgTRPPL-2 is able to conduct cation currents and to determine if the activity measured could be the result of permeation of potassium, we replaced potassium with the non-permeable ion cesium [33, 34]. In the presence of 1.8 mM Ca^{2+} inside the pipette, in a cesium chloride solution, membranes from TgTRPPL-2 and PC2 expressing cells have a significantly higher activity than control cells (Fig. 5A). The current-voltage relationship is linear through different applied voltages and significantly different from that of control cells in potassium or cesium chloride solution (Fig. 5B). Although channel conductance is slightly higher in potassium chloride, it is not significantly different than the calculated conductance and open probability obtained in Cesium chloride (Fig. 5B-C). However, when applying voltages higher than -40 mVs, the channel was open for longer times in the presence of cesium chloride vs potassium chloride (Fig. 5D, *green vs. blue line*). These results indicate that TgTRPPL-2 permeates Ca^{2+}, however it can also conduct potassium, since channel conductance is slightly higher in the potassium chloride solution.

We further demonstrate that TgTRPPL-2 is able to conduct Ca^{2+} by following Ca^{2+} changes of TgTRPPL-2-HEK-3KO or RFP-ER-HEK-3KO cells co-transfected with a genetic Ca^{2+} indicator, allowing to measure ER luminal Ca^{2+} changes and current activity simultaneously. Luminal Ca^{2+} changes were followed through one cycle of membrane depolarization from -80 mV to 40 mV (Fig. S4A). The fluorescence of the Ca^{2+} indicator decreased in the TgTRPPL-2 expressing cells

with time as voltage was applied. In both potassium as well as cesium chloride solutions at 1.8 mM Ca^{2+} we observed that the fluorescence decrease was significantly larger when the HEK-3KO cells expressed *TgTRPPL-2* (Fig. S4B-C vs. D-E). The slope for the fluorescence decrease appeared higher in the cesium chloride solution than in the potassium solution, although was quite variable (Fig. S4F-G). In summary, the observed decrease in the fluorescence of the Ca^{2+} indicator supports the Ca^{2+} permeation activity of TgTRPPL-2, which agrees with the single channel conductance measurements.

Inhibition of TgTRPPL2 by TRP Channel Inhibitors

Previous results from our laboratory demonstrated Ca^{2+} influx in *T. gondii* and its inhibition by L-type voltage gated Ca^{2+} channel blockers like nifedipine (Fig. 6A) [8]. Taking into account that TgTRPPL-2 is a cation permeable channel and localizes to the PM, we next investigated if the residual Ca^{2+} influx activity observed with the *ΔTgTRPPL-2* mutants could be blocked with nifedipine. Interestingly, pre-incubation with nifedipine of the *ΔTgTRPPL-2* parasites showed that the initial cytosolic Ca^{2+} was elevated and it was around ~400 nM (compared to 100 nM of the parental strain under identical conditions) in Ca^{2+}-free buffer (Fig. 6B). Further addition of extracellular Ca^{2+} did not result in Ca^{2+} influx and only a slow steady cytosolic Ca^{2+} increase was observed (Fig. 6B). We attribute the higher cytosolic Ca^{2+} in the presence of nifedipine to leakage of stored Ca^{2+} into the cytosol as the cell is trying to compensate for the complete absence of Ca^{2+} influx. However, the lack of Ca^{2+} influx after adding extracellular Ca^{2+}, with almost 100% inhibition, points to a role for TgTRPPL-2 in Ca^{2+} influx and addition of nifedipine resulted in complete loss of Ca^{2+} influx.

We next tested the effect of anthranilic acid (ACA), a wide spectrum TRP channel inhibitor [35], on Ca^{2+} influx of both parental controls and *ΔTgTRPPL-2* mutants (Fig. 6C). ACA inhibited Ca^{2+} influx by 40-50% of the parental cell line (Fig. 6C, *black vs. red tracing*). However, preincubation of ΔTgTRPPL-2 tachyzoites with ACA, did not further reduce Ca^{2+} influx (Fig. 6C, *dark blue vs. light blue tracings*). Sensitivity to both nifedipine and ACA was restored in the complemented cell line (Fig. 6D). These results point to TgTRPPL-2 as a PM channel that conducts Ca^{2+}, and it is relevant for its influx from the extracellular milieu, and is sensitive to TRP channel inhibitors.

The Role of TRPPL-2 as a Ca^{2+} leak channel at the ER membrane

The dual localization of TgTRPPL-2 at the PM and ER indicates the potential function of the channel at both locations (Fig. 1D). Efflux of Ca^{2+} to the cytosol is observed after inhibiting the TgSERCA with Thap [36]. We tested the effect of ACA in ER Ca^{2+} efflux, and observed that incubation of tachyzoites of the parental strain with ACA, significantly decreased the efflux of Ca^{2+} caused by Thap (Fig. 6 E-F, *black line and bar vs. red line and bar*). The ACA inhibited ER Ca^{2+} efflux rate was comparable to the decreased efflux rate triggered by Thap of the *ΔTgTRPPL-2* mutants (Fig. 6F, *blue bar versus red bar and* Fig. 3D). In addition, Ca^{2+}-activated Ca^{2+} entry, evaluated by adding 1.8 mM of extracellular Ca^{2+} 50 s after stimulating efflux with Thap, was

inhibited by ACA (Fig. 6G, *green versus gold line*). Ca^{2+} influx after Thap was reduced to basal Ca^{2+} influx (without pre-addition of Thap) for both parental and *ΔTgTRPPL-2* mutants. Note that Ca^{2+} influx in *ΔTgTRPPL-2* tachyzoites after stimulus by Thap, and Ca^{2+} influx in the parental strain without any stimulus are similar because the modulation of Ca^{2+} influx by cytosolic Ca^{2+} is lost in the *ΔTgTRPPL-2* parasites (Fig. 6H, *black versus blue bars*). In conclusion, ACA inhibited both efflux of Ca^{2+} from the ER as well as Ca^{2+}-induced Ca^{2+} entry. This led us to propose that TgTRPPL-2, in addition to mediate Ca^{2+} influx at the plasma membrane may also mediate Ca^{2+} leakage from the ER, a pathway sensitive to the TRP-channel inhibitor ACA.

To further validate the specificity of ACA for the inhibition of TgTRPPL-2, we tested this inhibitor and a second broad spectrum TRP channel inhibitor, benzamil, against single channel conductance. Channel activity of TgTRPPL-2 was significantly decreased by both ACA and benzamil (Fig. 7A-B). ACA diminished the amplitude of the channel by reducing the probability and time that the channel remained open (Fig. 7C, E). Conductance of the channel was reduced to almost half in the presence of ACA (Fig. 7B), which correlates with the inhibition of Ca^{2+} entry in *T. gondii*. In comparison to ACA, benzamil only reduced the open probability of TgTRPPL-2 but not the length of time the channel was open (Fig. 7D-E)). The conductance of TgTRPPL-2 was reduced to one third of the control in the presence of benzamil (Fig. 7B).

Most interesting, we tested both inhibitors, ACA and benzamil in *in vitro* growth assays (Fig. 7F-G, *top panel and parental bars*) and found that they both inhibited *in vitro T. gondii* growth. We calculated the IC_{50} for ACA at 1.4 ± 0.4 μM. Interestingly, neither ACA nor benzamil affected the growth of the *ΔTgTRPPL*-2 mutants (Fig. 7G). Note that these cells already grow at a slower rate, which did not change in the presence of the inhibitors. However, cilnidipine, a voltage-gated Ca^{2+} channel blocker, completely inhibited growth of both parental and *ΔTgTRPPL*-2 mutants (Fig. 7G).

In conclusion, TgTRPPL-2 is a cation permeable channel that can be inhibited by broad spectrum TRP channel inhibitors. Inhibition of channel activity affects parasite growth.

DISCUSSION

In this study we report the presence and functional role of a *T. gondii* channel, TgTRPPL-2, that localizes to the plasma membrane and the endoplasmic reticulum. The corresponding gene *TgGT1_310560*, was annotated as hypothetical but was predicted as a transient receptor potential channel based on a bioinformatic analysis of the *T. gondii* genome comparing it with TRP channel genes of mammalian origin [17]. Here, we established that TgTRPPL-2 is important for both Ca^{2+} influx at the PM and Ca^{2+} efflux from the ER of *T. gondii* tachyzoites. TgTRPPL-2, expressed in HEK-3KO cells, conducted currents in high calcium solutions and was not voltage dependent. Interestingly, Ca^{2+} itself modulated the conductance of TgTRPPL-2. Broad spectrum TRP channel inhibitors like ACA and benzamil, inhibited the activity of TgTRPPL-2, Ca^{2+} influx in the parasite as well as parasite growth.

Silencing of TgTRPPL-2 in the *ΔTgTRPPL-2* mutants impacted both invasion and egress of *T. gondii*, resulting in a general growth defect. Extracellular tachyzoites, which are surrounded by high Ca^{2+} are able to use Ca^{2+} influx to stimulate invasion of a new host cell and carry on their lytic cycle. The *ΔTgTRPPL-2* mutants showed a reduction in their host invasion ability suggesting the defect may be due to a reduction in Ca^{2+} influx because of the absence of TgTRPPL-2. Interestingly, the reduction in Ca^{2+} influx (~50%) in the *ΔTgTRPPL-2* mutants was comparable to the reduction of invasion suggesting that TgTRPPL-2 is involved in the Ca^{2+} influx pathway that stimulates invasion. Delay in the ability of the *ΔTgTRPPL-2* mutants to egress could be caused by a defective efflux of Ca^{2+} from the ER, which was significantly lower in the mutants. This was evidence for the function of TgTRPPL2 as a Ca^{2+} channel at the ER membrane.

The impact of silencing TgTRPPL-2 on *T. gondii* growth, was not total and parasites still were able to perform lytic cycle activities at a reduced rate. The main defects of the *ΔTgTRPPL-2* mutants: invasion, egress, Ca^{2+} influx and ER Ca^{2+} efflux was not complete likely because more than one mechanism or channel is functional at both locations (PM and ER). We hypothesize the presence of another channel at the PM, likely the one responsible for the Ca^{2+} influx activity that is inhibited by nifedipine [8]. It is also possible that a release channel responsive to IP_3 may be involved in release of Ca^{2+} from the ER [37] with TgTRPPL-2 having a role in efflux under conditions of ER Ca^{2+} overload.

Numerous observations in *T. gondii* have demonstrated that intracellular Ca^{2+} oscillations in the parasite precede the activation of distinct steps of the lytic cycle [6, 7]. Influx of both extracellular and intracellular Ca^{2+} pools into the parasite cytosol contribute to the activation of downstream signaling pathways decoded into critical biological steps of the parasite lytic cycle [7, 38]. Ca^{2+} influx at the plasma membrane of *T. gondii* is highly regulated, stimulated by cytosolic Ca^{2+} and is operational in extracellular [8] and intracellular replicating tachyzoites [9]. Our data with the *ΔTgTRPPL-2* cells identified TgTRPPL-2 as a functional protein at the plasma membrane and the ER and in both locations would allow Ca^{2+} influx into the cytosol. The dual localization of TgTRPPL-2 is in accord with other TRP channels in other cells, which showed a dynamic localization between vesicular organelles and the plasma membrane where they facilitate Ca^{2+} influx [39]. In this regard, the mammalian ortholog, PC2, localizes to both the plasma membrane and the ER [40].

T. gondii expresses a SERCA-Ca^{2+}-ATPase, a P-type ATPase, that couples ATP hydrolysis to the transport of ions across biological membranes (TgSERCA) and localizes to the ER [41]. TgSERCA is sensitive to thapsigargin (Thap), a sesquiterpene lactone derived from the plant *Thapsia garganica* [42, 43] and previous studies showed that inhibition of TgSERCA by Thap resulted in cytosolic Ca^{2+} efflux through an unknown channel [8, 36]. In mammalian cells, the passive Ca^{2+} efflux from the ER is thought to prevent ER Ca^{2+} overload and helps maintain the steady-state concentration of luminal Ca^{2+} permitting cytosolic Ca^{2+} signaling [2, 44]. Several membrane proteins have been proposed to be involved in the ER Ca^{2+} efflux/leak pathway including TRP channels [45]. Results from this work support a role for TgTRPPL-2 in ER Ca^{2+} leakage in *T. gondii*. Ca^{2+} efflux from the ER observed after adding Thap or Zaprinast was also

significantly decreased in the *ΔTgTRPPL-2* mutants. These results support a functional role for TgTRPPL-2 at the membrane of the ER as the constitutive leak channel involved in Ca^{2+} efflux when the store is filled. This could also be the mechanism by which the ER supplies Ca^{2+} to other organelles like the mitochondria or the plant-like vacuole (PLV) a lysosome like compartment [46].

Previous work from our laboratory showed that Ca^{2+} influx at the plasma membrane did not operate as store-operated Ca^{2+} entry (SOCE) which was shown with experiments testing surrogate ions like Mn^{2+} [8]. This result was supported by the lack of components of the SOCE pathway, STIM and ORAI from the *T. gondii* genome [17]. However, Ca^{2+} influx was modulated by cytosolic Ca^{2+} [8] and this modulation was absent in the *ΔTgTRPPL-2* cells supporting a role for TgTRPPL-2 as the channel responsible for Ca^{2+} influx at the PM activated by cytosolic Ca^{2+}. TRP channels have been shown to play a role in Ca^{2+}-activated Ca^{2+} entry [47]. Release of Ca^{2+} from intracellular stores like the ER, is also significantly diminished in the *ΔTgTRPPL-2* mutants, which could affect the stimulation of Ca^{2+} influx. However, when using Zaprinast, which raised cytosolic Ca^{2+} at a much higher level than Thap, the stimulation of Ca^{2+} influx by cytosolic Ca^{2+} was absent. This further supports that TgTRPPL-2 functions at the PM mediating Ca^{2+} influx and is modulated by cytosolic Ca^{2+}.

We showed that TgTRPPL-2 was able to conduct currents with conductance values comparable to the values of mammalian TRP channels [48-50]. Previous work with PC2, showed that Ca^{2+} modulated the activity of PC2 [51-53] [48, 54]. Sustained cytosolic Ca^{2+} increase inhibited PC2 currents [53] while other studies showed that cytosolic Ca^{2+} increase from physiological (100 nM) to μM levels increased the activity of the channel [48, 54]. We observed some of these responses with TgTRPPL-2, as increasing Ca^{2+} inside the pipette (ER luminal) showed a significant decrease in the currents. Comparably, increasing Ca^{2+} concentration in the bath solution (cytosolic) from physiological levels to μM levels showed an increase of 2.5x in the conductance of TgTRPPL-2. Although cytosolic [Ca^{2+}] is unlikely to reach those high μM levels, the potential presence of Ca^{2+} microdomains at the plasma membrane or the ER membrane would result in higher concentrations of Ca^{2+} at the exit of the channel due to slow diffusion of Ca^{2+} ions [55-57].

Because PKD channels are cation permeable they could also permeate Na^{+} or K^{+}. In the case of TgTRPPL-2 we showed that it can mediate Ca^{2+} transport when no other ions are present in the solution. We did not determine the ionic selectivity of TgTRPPL-2, and we can only propose that TgTRPPL-2 is a cation permeable channel. In cilia, PKD channels have been described to have relatively high conductance [48, 58]. The conductance calculated for TgTRPPL-2 is within range of what has been described for PC2 in other cells (30-157 pS). However, it is important to note that the properties described for any channel will depend on the experimental approaches used.

Anthranilic acid and benzamil are broad spectrum inhibitors that have the ability to inhibit TRP channel activity. ACA is a weak base that inhibits currents mediated by TRP channels. ACA does not block the pore of the channel as most inhibitors but rather reduce the open probability of the channel. In a similar manner, benzamil is also able to inhibit currents mediated by TRP channels

by binding to a site that modulates their activity rather than blocking its pore. In our experiments testing ACA and benzamyl we observed that while the inhibitors affected Ca^{2+} influx and growth of the parental cell line, neither affected the already reduced growth and Ca^{2+} influx of the *ΔTgTRPPL-2* mutants. This result combined with the inhibition of TgTRPPL-2 currents impacting both open probability and time that the channel remained open points to TgTRPPL-2 as the target of ACA and benzamyl.

Recent studies on Ca^{2+} signaling in *T. gondii* have expanded our understanding of the link between Ca^{2+} and critical facets of parasite biology (i.e., gliding motility, microneme secretion, host cell invasion and egress). However, important molecular players have remained enigmatic, like the PM channels responsible for Ca^{2+} influx and the ER channel responsible for the passive leakage into the cytosol. Characterization of TgTRPPL-2 and its function at the ER and PM fills a small gap in our knowledge of Ca^{2+} signaling and homeostasis in *T. gondii* (Fig. 8). This study is the first biophysical characterization of a channel in *T. gondii* (or any Apicomplexan parasite) and TgTRPPL-2 represents the first identified molecule to mediate Ca^{2+} influx into the cytosol of *T. gondii* at the plasma membrane and the ER. In addition, this study identifies TgTRPPL-2 as a potential target for combatting Toxoplasmosis.

EXPERIMENTAL PROCEDURES

Toxoplasma growth

All parasite strains were continuously maintained *in vitro* by serial passage in Dulbecco's modified minimal essential media (DMEM) with 1% FBS, 2.5 μg/ml amphotericin B, 100 μg/ml streptomycin in the human telomerase reverse transcriptase immortalized foreskin fibroblasts (hTERT) [59].

Generation of mutants

The smHA-LIC-CAT plasmid was used for *in situ* C-terminal tagging of TgTRPPL-2-smHA [19]. Carboxy-terminus tagging was done in the parental line RHTatiΔku80 (TatiΔku80) [23] a parasite line that contains the tetracyclin-regulated transactivator system that allows conditional expression of genes [60] and also in which the *ku80* gene was deleted increasing efficiency of homologues recombination [61]. Briefly, a homology region of 974 bp covering the 3' region of the gene of interest excluding the STOP codon was amplified by PCR using *T. gondii* RH genomic DNA as template and cloned into the plasmid. Plasmids were validated by restriction digest and sequencing. The oligonucleotides primers used for PCR and for creating the gene-tagging plasmids and for PCR validations are listed in Table S3 (Primers T1-T3). Prior to transfection all plasmids were linearized within the region of homology. Approximately 20 µg of plasmid DNA was used for transfection of $1x10^7$ *T. gondii* RHTatiΔKu80 parasites using a Gene Pulser X Cell electroporator (BioRad). Selection was done with 20 µM chloramphenicol, and clones were isolated by limiting dilution. DNA of selected clones were isolated and screened by PCR.

To disrupt the *TgTRPPL-2* (TgGT1_310560) gene a single guide RNA against TgTRPPL-2 was constructed as described [62]. The single guide RNA was mutagenized with the desired

sequence in a plasmid that contains the Cas9 using the Q5 Mutagenesis Kit following manufacturer's instructions. The correct mutation was verified by sequencing. The pyrimethamine-resistant DHFR cassette was amplified by PCR with primers containing 50 bp homology arms of the region upstream and downstream of the start and stop codon of the *TgTRPPL-2* gene. The created sgTgTRPPL-2 CRISPR plasmid was co-transfected with the DHFR cassette (3:1 respectively) into RH tachyzoites. Selection followed with pyrimethamine for 7 days. Parasites were sub-cloned by limiteing dilution and screening for clones was done by PCR. The primers used for the creation of the ΔTgTRPPL-2 are listed in Table S3 (Primer K1-K4).

Quantitative PCR. Total RNA from parental, *ΔTgTRPPL-2* and *ΔTgTRPPL2-trppl2* was extracted and reversed-transcribed into cDNA. The qPCR reaction was done using the iQ™SYBR Green master mix (BioRad), plus primers, and the reverse-transcribed cDNA (Primers shown in Table S3, Q1-Q2). The qRT-PCR was carried out on a CFX96™ PCR Real-Time detection system (C1000Touch™ Thermal cycler, BioRad). Relative quantification software (CFX Maestro™ software) was used for the analysis and relative expression levels were calculated as the fold change using the formula $2^{\Delta\Delta}$CT [63]. Normalization was done using Actin and Tubulin primers. Experiments were repeated three times with triplicate samples.

Antibody production of TgTRPPL-2. The antigenic region for TgTRPPL-2 chosen for antibody production was identified using the IEDB suite of antigenicity prediction software. The DNA sequence was amplified from RH genomic DNA and cloned into the pET-32 LIC/EK vector (Novagen), which adds an N-terminal thioredoxin and histidine tag to the expressed protein. Recombinant CP1Ag was expressed and initially purified via a nickel-affinity column (HisPur Thermo Fisher) as previously described [64]. Cleavage of the N-terminal thioredoxin and histidine tag was done by biotinylated thrombin. The antigen was passed again through the nickel column and the purified tag-less antigen was gently eluted using 10 mM imidazole. Antibodies in mice were generated as previously [65]. Swiss Webster mice (Charles River) were inoculated intraperitoneally with 100 µg of TgTRPPL-2 mixed with complete Freund's adjuvant, followed by two boosts with 50 µg of TgTRPPL-2 in incomplete Freund's adjuvant. The final serum was collected by cardiac puncture after CO_2 euthanasia. We created a αSERCA antibody for co-localization studies of the TgTRPPL-2. The phosphorylation (P) and nucleotide binding (N) domains of *Tg*SERCA were cloned into XmaI and HindIII sites of pQE-80L plasmid for expression in *Escherichia coli* BL21-CodonPlus competent cells. Purified antigen was used to immunize Guinea pigs with 0.2 mg of antigen mixed with Freund's Complete Adjuvant, followed by two boosts of 0.1 mg antigen mixed with Freund's Incomplete Adjuvant (Sigma F5506). The resulting antibodies were used at 1:1,000 for western blots. The animal protocol used was approved by the UGA Institutional Animal Care and Use Committee (IACUC).

Western blot analysis. SDS-polyacrylamide gel electrophoresis (SDS-PAGE) followed established protocols [66]. Lysates were prepared by resuspending a pellet of 1 x 10^8 tachyzoites

in 50 µL of Cell Lytic^{M} lysis buffer containing 12.5 U benzonase and 1 X protease cocktail inhibitor (P8340 Sigma). The reaction was stopped with one volume of 2% SDS and 1 mM EDTA. Total lysates were boiled in Laemmli sample buffer (BioRad). Immunoblotting followed established protocols using mouse anti-HA monoclonal antibody (1:1,000) (Roche). Detection was done using the Odyssey Clx LICOR system using goat anti-mouse IRDye800WC (1:10,000). Loading control for westerns were done with primary mouse-anti-tubulin antibodies at a 1:15,000 dilution and goat anti-mouse IRDDye800WC as secondary (1:10,000).

Immunofluorescence microscopy Extracellular parasites were collected and purified as previously [67]. Parasites were washed once with buffer A with glucose (BAG, 116 mM NaCl, 5.4 mM KCl, 0.8 mM $MgSO_4$, 5.5 mM glucose and 50 mM HEPES, pH 7.4) and an aliquot of 2 x 10^4 parasites was overlaid on a coverslip previously treated with poly-L-Lysine. Intracellular tachyzoites were grown on hTERT cells on coverslips. Both extracellular and intracellular parasites were fixed with 3% paraformaldehyde for 20 min at room temperature (RT), permeabilized with 0.3% Triton X-100, blocked with 3% bovine serum albumin (BSA), and exposed to primary antibodies (Ratα-HA 1:100). The secondary antibodies used were goat-αrat Alexa Fluor 488 (Life Technologies) at a 1:1,000 dilution. For co-localization studies we used α-Sag1 (1:1,000) as membrane marker and α-TgSERCA as ER marker (1:1,000). Slides were examined using an Olympus IX-71 inverted fluorescence microscope with a photometric CoolSNAP HQ charge-coupled device (CCD) camera driven by DeltaVision software (Applied Precision, Seattle, WA).

Immunoprecipitation assays. Freshly lysed tachyzoites expressing TgTRPPL-2-smHA were collected and filtered through an 8 μM membrane (Whatman). Tachyzoites were washed twice in BAG and resuspended in lysis buffer (50mM Tris-HCl, pH 7.4, 150 mM KCl, 1 mM EDTA, 0.4% NP-40) to a final concentration of 2 x 10^9 total cells. Lysis was allowed to proceed for thirty minutes at 4^{o}C and cells were centrifuged at 15,000 x g for 20 min. Immunoprecipitation of TgTRPPL-2-smHA protein was performed using the Pierce HA Tag/Co-IP Kit (Thermo Fisher Scientific, Waltham, MA) according to manufacturer's instructions. Briefly, HA magnetic beads were washed twice in lysis buffer and mixed with the parasite lysate by vortexing for 1 h at RT. Beads were collected and the flow-through fraction was saved for further analysis. Beads were washed twice in wash buffer (50mM Tris-HCl, pH 7.4, 150 mM KCl, 1 mM EDTA, 0.1% NP-40) and once in ddH_2O by gentle mixing. The tagged protein was recovered by mixing the beads with 1x Laemmli buffer and heated at 65^{o}C for 10 min. The supernatant was collected and used for PAGE and western blots. The corresponding band was cut and resuspended in water and analyzed using LC-Mass Spectrometry. Samples were sent to the Proteomics and Mass Spectrometry Core Facility at the University of Georgia for analysis. The average counts that were obtained from two biological samples are shown in Table S2. Proteins with counts higher than 3 are shown.

Growth and Invasion Assays. Plaque assays were done as previously described, with slight modifications [67]. Briefly, 200 egressed tachyzoites were allowed to infect confluent hTERT cells for 7 days. After seven days cells were fixed with ethanol and stained with crystal violet. Plaque sizes were analyzed using FIJI [68]. Invasion assay were performed as previously described, with slight modifications [28]. A subconfluent monolayer of HFF cells were infected with $2x10^7$ tachyzoites in the presence of 1.8 mM or 0.5 mM Ca^{2+} and placed for 20 minutes on ice and subsequently transferred for 5 minutes to a 37°C water bath for parasite invasion. Cells were immediately fixed with 3% paraformaldehyde for 20 minutes. Extracellular parasites (attached) were stained using RabbitαSag1 (1:1,000) prior to permeabilization while intracellular parasites (invaded) were stained with MouseαSag1 (1:200). Secondary antibodies were goat-αrabbit Alexa Fluor 546 (1:1,000) and goat-αmouse Alexa Fluor 488 (1:1,000). Images were taken with an Olympus IX-71 inverted fluorescence microscope with a Photometric CoolSNAP HQ CCD camera driven by DeltaVision software (Applied Precision, Seattle, WA). Quantification was made of ten-fields of view at a 1000 magnification from three independent biological replicates. Percentage of invaded vs attached was quantified by dividing the number of parasites invaded or attached by the total parasites quantified in the field of view.

Egress experiments. hTERT cells were infected with $5x10^5$ of RH or ΔTgTRPPL-2 tachyzoites. 24 h after infection parasitophorous vacuoles were observed by microscopy and washed with Ringer's buffer (155 mM NaCl, 3 mM KCl, 1 mM MgCl2, 3 mM $NaH_2PO_4H_2O$, 10 mM HEPES, pH 7.3, and 5 mM glucose). Ringer's buffer was used as extracellular buffer in the presence or absence of 1.8 mM Ca^{2+}. Drugs were added in Ringer's buffer 30 sec after imaging at the following concentrations: saponin (0.02%) or Zaprinast (100 μM). Images were acquired in a time-lapse mode with an acquisition rate of 3 seconds for 12-20 minutes. For statistical analysis, egress time was quantified as the first parasite to egress out of the parasitophorous vacuole. Statistical analysis was done for 3 independent biological replicates and at least 5 PVs per experiment.

Cytosolic Ca^{2+} measurements. Parasites were loaded with Fura2-AM as described in [36]. Briefly, fresh lysed parasites were washed twice at 1,800 rpm for 10 min at room temperature in buffer A (BAG) (116 mM NaCl, 5.4 mM KCl, 0.8 mM MgSO4, 5.5 mM d-glucose and 50 mM Hepes, pH 7.4). Parasites were resuspended to a final density of $1x10^9$ parasites/mL in loading buffer (Ringer's plus 1.5% sucrose, and 5 μM Fura2-AM). The suspension was incubated for 26 min at 26 °C with mild agitation. Subsequently, the parasites were washed twice with Ringer's buffer to remove extracellular dye. Parasites were resuspended to a final density of $1x10^9$ parasites/mL in Ringer's buffer and kept in ice. For fluorescence measurements, $2x10^7$ parasites/mL were placed in a cuvette with 2.5 mL of Ringer's buffer. The cuvette was placed in a thermostatically controlled Hitachi F-7000 fluorescence spectrophotometer. Excitation was at 340 and 380 nm, and emission at 510 nm. The Fura2-AM fluorescence relationship to intracellular Ca^{2+} concentration ($[Ca^{2+}]_i$) was calibrated from the ratio of 340/380 nm fluorescence values after subtraction of the background fluorescence of the cells at 340 and 380 nm as previously described [69]. Changes in

$[Ca^{2+}]_i$ (ΔF $[Ca^{2+}]$) were measured by subtracting the highest peak of Ca^{2+} in the first 20 s after addition of Ca^{2+} or 100 s after the addition of drugs minus the baseline.

Cell transfections and culture of HEK-3KO Cells.

Total RNA of wild type *T. gondii* were extracted and reversed transcribed into cDNA. TgTRPPL-2 whole cDNA was amplified using primers shown in Table S3 (Primers C1-C6). The amplified cDNA was cloned into the Zero Blunt TOPO vector using the cloning kit per manufacturers instruction. Correct insertion was verified by colony PCR using M13F and M13R primers. Restriction digests was performed to remove the insert from the vector using the following restriction enzymes: BamHI and AvrII. The purified *TgTRPPL-2 cDNA* was ligated to linearized pCDNA 3.1 plasmid. Ligation to the vector was confirmed by PCR and sequencing. Purified TRPPL-2-pCDNA was used to co-transfect DT40-3KO cells.

HEK cells which have the 3 endogenous isoforms of the IP_3 receptor knocked out were a gift from Dr. David Yule [31, 70]. The cells were maintained in Dulbecco's modified minimal essential media (DMEM) with 10% Fetal Bovine Serum 2.5 μg/ml amphotericin B and 100 μg/ml streptomycin. Cells were transiently transfected as previously described [71] with 2.5 µg of TgTRPPL-2, PC2 or RFP DNA targeted to the ER. Each plasmid DNA were diluted in 200 µL of Opti-MEM with 25 µL of polyethylenimine and incubated for 10 min. The mix was then added to semi confluent HEK-3KO cells in a dropwise manner, and 24 h later the media was changed.

Preparation of Nuclear extracts. 48 hours after transfection, cells were collected and the nucleus extracted as previously described [72]. $2x10^7$ of transiently transfected cells were collected in ice cold PBS. Cells were spun down and washed twice in PBS and resuspended in Nuclei Isolation Solution (150 mM KCl, 250 mM Sucrose, 10 mM Tris-HCl, 1.4 mM β-mercaptoethanol, 0.2 mM PMSF, pH 7.3). Cells were homogenized with a homogenizer and stored on ice. 100 µL of nuclei were transferred to cover slips previously coated with poly-L-lysine and incubated for 20 minutes before filling the chamber with bath solution.

Patch clamp of Nuclear membranes. Nuclear extract expressing TgTRPPL-2 or the control gCaMPER [73] were used for analysis. Electrical currents were recorded using Standard Wall Borosilicate Capillaries (Harvard Bioscience, Massachusetts) with 10-15 MΩ resistance. Holding potentials were maintained at 0 mV. The internal solution contained: 140 mM KCl or CsCl, 10 mM HEPES, 1.8 mM or 10 mM free Ca^{2+} adjusted with EGTA. Standard Bath Solution contained the same reagents and concentrations as the pipette solution using 100 nM of free Ca^{2+}. The single-channel conductance was obtained from the current-voltage relationship for each condition tested. Ca^{2+} currents were elicited by applying pulses from -80 mV up to 20 mV for 25 seconds. Analysis of amplitude, open probability and channel conductance were done using a 45 kHz filter. Data for recording was collected using the HEKA Electronic Patch Clamp EPC10 (Harvard Bioscience, Massachusetts).

Statistics. Statistical analyses were performed by Student's *t-test* using GraphPad PRISM version 8.2. All experimental data were analyzed from at least three independent biological replicates. Error bars shown represent standard error of the mean (SEM) of the biological replicates analyzed. For the electrophysiological analysis a total of 3 cells per biological replicate (9 total cells) were analyzed. Each cell was depolarized a total of 5 times per experimental conditions.

Acknowledgements*:* We thank Drs. David Yule for providing the HEK-3KO cells for electrophysiological analyses, John Boothroyd for antibodies against SAG1 and Boris Striepen for providing us with the Cosmid for complementation. Catherine Li prepared the antigen used to generate the anti-SERCA antibody. The super resolution microscope is part of the Biomedical Microscopy Core (BMC) of the University of Georgia. We thank the University of Georgia Graduate School for awarding a Summer Research Travel Grant to KMMN. This work was supported by the U.S. National Institutes of Health grant AI128356 to SNJM and R00 DK101585 to IYK. KMMN was partially supported through a fellowship funded by a T32 training grant, 5T32AI060546.

Author Contributions

KMMN, performed and coordinated most of the experiments, analyzed the data, wrote the manuscript; **NC**, developed the specific antibody and contributed to its validation; **MAHT**, developed the knockout strain and its validation; **IK**, writing, review, editing, analysis and interpretation of data; **SNJM**, coordinated the project and experiments, contributed resources and wrote the manuscript.

References

1. Berridge MJ, Bootman MD, Roderick HL. Calcium signalling: dynamics, homeostasis and remodelling. Nat Rev Mol Cell Biol. 2003;4(7):517-29. Epub 2003/07/03. doi: 10.1038/nrm1155. PubMed PMID: 12838335.
2. Clapham DE. Calcium signaling. Cell. 2007;131(6):1047-58. doi: 10.1016/j.cell.2007.11.028. PubMed PMID: 18083096.
3. Blader IJ, Coleman BI, Chen CT, Gubbels MJ. Lytic Cycle of Toxoplasma gondii: 15 Years Later. Annu Rev Microbiol. 2015;69:463-85. Epub 2015/09/04. doi: 10.1146/annurev-micro-091014-104100. PubMed PMID: 26332089; PubMed Central PMCID: PMCPMC4659696.
4. Weiss LM, Dubey JP. Toxoplasmosis: A history of clinical observations. Int J Parasitol. 2009;39(8):895-901. Epub 2009/02/17. doi: 10.1016/j.ijpara.2009.02.004. PubMed PMID: 19217908; PubMed Central PMCID: PMCPMC2704023.
5. Black MW, Boothroyd JC. Lytic cycle of Toxoplasma gondii. Microbiol Mol Biol Rev. 2000;64(3):607-23. PubMed PMID: 10974128.
6. Lourido S, Moreno SN. The calcium signaling toolkit of the Apicomplexan parasites Toxoplasma gondii and Plasmodium spp. Cell Calcium. 2015;57(3):186-93. Epub 2015/01/22. doi: 10.1016/j.ceca.2014.12.010. PubMed PMID: 25605521; PubMed Central PMCID: PMCPMC4428288.
7. Hortua Triana MA, Marquez-Nogueras KM, Vella SA, Moreno SNJ. Calcium signaling and the lytic cycle of the Apicomplexan parasite Toxoplasma gondii. Biochim Biophys Acta Mol Cell Res. 2018;1865(11 Pt B):1846-56. Epub 2019/04/18. doi: 10.1016/j.bbamcr.2018.08.004. PubMed PMID: 30992126; PubMed Central PMCID: PMCPMC6477927.
8. Pace DA, McKnight CA, Liu J, Jimenez V, Moreno SN. Calcium entry in Toxoplasma gondii and its enhancing effect of invasion-linked traits. J Biol Chem. 2014;289(28):19637-47. Epub 2014/05/29. doi: 10.1074/jbc.M114.565390. PubMed PMID: 24867952; PubMed Central PMCID: PMCPMC4094074.
9. Vella SA, Moore, C. A., Li, Z., Hortua Triana, M.A., Potapenko, E., Moreno, S.N.J. The Role of Potassium and Host Calcium Signaling in Toxoplasma gondii egress. bioRxiv. 2020. doi: https://doi.org/10.1101/2020.03.06.980508.
10. Nilius B, Owsianik G. The transient receptor potential family of ion channels. Genome Biol. 2011;12(3):218. Epub 2011/03/16. doi: 10.1186/gb-2011-12-3-218. PubMed PMID: 21401968; PubMed Central PMCID: PMCPMC3129667.
11. Zhou J. Polycystins and primary cilia: primers for cell cycle progression. Annu Rev Physiol. 2009;71:83-113. Epub 2009/07/04. doi: 10.1146/annurev.physiol.70.113006.100621. PubMed PMID: 19572811.
12. Venkatachalam K, Montell C. TRP channels. Annu Rev Biochem. 2007;76:387-417. Epub 2007/06/21. doi: 10.1146/annurev.biochem.75.103004.142819. PubMed PMID: 17579562; PubMed Central PMCID: PMCPMC4196875.
13. Koulen P, Cai Y, Geng L, Maeda Y, Nishimura S, Witzgall R, et al. Polycystin-2 is an intracellular calcium release channel. Nat Cell Biol. 2002;4(3):191-7. Epub 2002/02/21. doi: 10.1038/ncb754. PubMed PMID: 11854751.
14. Samanta A, Hughes TET, Moiseenkova-Bell VY. Transient Receptor Potential (TRP) Channels. Subcell Biochem. 2018;87:141-65. Epub 2018/02/22. doi: 10.1007/978-981-10-7757-9_6. PubMed PMID: 29464560; PubMed Central PMCID: PMCPMC6038138.
15. Wang Z, Ng C, Liu X, Wang Y, Li B, Kashyap P, et al. The ion channel function of polycystin-1 in the polycystin-1/polycystin-2 complex. EMBO Rep. 2019;20(11):e48336. Epub 2019/08/24. doi: 10.15252/embr.201948336. PubMed PMID: 31441214; PubMed Central PMCID: PMCPMC6832002.

16. Wolstenholme AJ, Williamson SM, Reaves BJ. TRP channels in parasites. Adv Exp Med Biol. 2011;704:359-71. Epub 2011/02/04. doi: 10.1007/978-94-007-0265-3_20. PubMed PMID: 21290306.
17. Prole DL, Taylor CW. Identification of intracellular and plasma membrane calcium channel homologues in pathogenic parasites. PloS one. 2011;6(10):e26218. Epub 2011/10/25. doi: 10.1371/journal.pone.0026218. PubMed PMID: 22022573; PubMed Central PMCID: PMC3194816.
18. Boucher C, Sandford R. Autosomal dominant polycystic kidney disease (ADPKD, MIM 173900, PKD1 and PKD2 genes, protein products known as polycystin-1 and polycystin-2). Eur J Hum Genet. 2004;12(5):347-54. Epub 2004/02/12. doi: 10.1038/sj.ejhg.5201162. PubMed PMID: 14872199.
19. Hortua Triana MA, Marquez-Nogueras KM, Chang L, Stasic AJ, Li C, Spiegel KA, et al. Tagging of Weakly Expressed Toxoplasma gondii Calcium-Related Genes with High-Affinity Tags. J Eukaryot Microbiol. 2018;65(5):709-21. Epub 2018/04/20. doi: 10.1111/jeu.12626. PubMed PMID: 29672999; PubMed Central PMCID: PMCPMC6175649.
20. Montell C. The TRP superfamily of cation channels. Sci STKE. 2005;2005(272):re3. Epub 2005/02/25. doi: 10.1126/stke.2722005re3. PubMed PMID: 15728426.
21. Omasits U, Ahrens CH, Muller S, Wollscheid B. Protter: interactive protein feature visualization and integration with experimental proteomic data. Bioinformatics. 2014;30(6):884-6. Epub 2013/10/29. doi: 10.1093/bioinformatics/btt607. PubMed PMID: 24162465.
22. Soding J. Protein homology detection by HMM-HMM comparison. Bioinformatics. 2005;21(7):951-60. Epub 2004/11/09. doi: 10.1093/bioinformatics/bti125. PubMed PMID: 15531603.
23. Sheiner L, Demerly JL, Poulsen N, Beatty WL, Lucas O, Behnke MS, et al. A systematic screen to discover and analyze apicoplast proteins identifies a conserved and essential protein import factor. PLoS Pathog. 2011;7(12):e1002392. Epub 2011/12/07. doi: 10.1371/journal.ppat.1002392. PubMed PMID: 22144892; PubMed Central PMCID: PMCPMC3228799.
24. Shen PS, Yang X, DeCaen PG, Liu X, Bulkley D, Clapham DE, et al. The Structure of the Polycystic Kidney Disease Channel PKD2 in Lipid Nanodiscs. Cell. 2016;167(3):763-73 e11. Epub 2016/10/22. doi: 10.1016/j.cell.2016.09.048. PubMed PMID: 27768895; PubMed Central PMCID: PMCPMC6055481.
25. Su Q, Hu F, Liu Y, Ge X, Mei C, Yu S, et al. Cryo-EM structure of the polycystic kidney disease-like channel PKD2L1. Nat Commun. 2018;9(1):1192. Epub 2018/03/24. doi: 10.1038/s41467-018-03606-0. PubMed PMID: 29567962; PubMed Central PMCID: PMCPMC5864754.
26. Merrick D, Bertuccio CA, Chapin HC, Lal M, Chauvet V, Caplan MJ. Polycystin-1 cleavage and the regulation of transcriptional pathways. Pediatr Nephrol. 2014;29(4):505-11. Epub 2013/07/05. doi: 10.1007/s00467-013-2548-y. PubMed PMID: 23824180; PubMed Central PMCID: PMCPMC3844055.
27. Vinayak S, Brooks CF, Naumov A, Suvorova ES, White MW, Striepen B. Genetic manipulation of the Toxoplasma gondii genome by fosmid recombineering. mBio. 2014;5(6):e02021. Epub 2014/12/04. doi: 10.1128/mBio.02021-14. PubMed PMID: 25467441; PubMed Central PMCID: PMCPMC4324243.
28. Kafsack BF, Beckers C, Carruthers VB. Synchronous invasion of host cells by Toxoplasma gondii. Mol Biochem Parasitol. 2004;136(2):309-11. Epub 2004/10/14. doi: 10.1016/j.molbiopara.2004.04.004. PubMed PMID: 15478810.
29. Petri ET, Celic A, Kennedy SD, Ehrlich BE, Boggon TJ, Hodsdon ME. Structure of the EF-hand domain of polycystin-2 suggests a mechanism for Ca2+-dependent regulation of polycystin-2 channel activity. Proc Natl Acad Sci U S A. 2010;107(20):9176-81. Epub 2010/05/05. doi: 10.1073/pnas.0912295107. PubMed PMID: 20439752; PubMed Central PMCID: PMCPMC2889120.
30. Sidik SM, Hortua Triana MA, Paul AS, El Bakkouri M, Hackett CG, Tran F, et al. Using a Genetically Encoded Sensor to Identify Inhibitors of Toxoplasma gondii Ca2+ Signaling. J Biol Chem. 2016;291(18):9566-80. Epub 2016/03/05. doi: 10.1074/jbc.M115.703546. PubMed PMID: 26933036; PubMed Central PMCID: PMCPMC4850295.

31. Alzayady KJ, Wang L, Chandrasekhar R, Wagner LE, 2nd, Van Petegem F, Yule DI. Defining the stoichiometry of inositol 1,4,5-trisphosphate binding required to initiate Ca2+ release. Sci Signal. 2016;9(422):ra35. Epub 2016/04/07. doi: 10.1126/scisignal.aad6281. PubMed PMID: 27048566; PubMed Central PMCID: PMCPMC4850551.
32. Celic A, Petri ET, Demeler B, Ehrlich BE, Boggon TJ. Domain mapping of the polycystin-2 C-terminal tail using de novo molecular modeling and biophysical analysis. J Biol Chem. 2008;283(42):28305-12. Epub 2008/08/13. doi: 10.1074/jbc.M802743200. PubMed PMID: 18694932; PubMed Central PMCID: PMCPMC2568934.
33. Almog M, Korngreen A. Characterization of voltage-gated Ca(2+) conductances in layer 5 neocortical pyramidal neurons from rats. PLoS One. 2009;4(4):e4841. Epub 2009/04/02. doi: 10.1371/journal.pone.0004841. PubMed PMID: 19337371; PubMed Central PMCID: PMCPMC2659773.
34. Wu LG, Westenbroek RE, Borst JG, Catterall WA, Sakmann B. Calcium channel types with distinct presynaptic localization couple differentially to transmitter release in single calyx-type synapses. J Neurosci. 1999;19(2):726-36. Epub 1999/01/09. PubMed PMID: 9880593; PubMed Central PMCID: PMCPMC6782194.
35. Harteneck C, Frenzel H, Kraft R. N-(p-amylcinnamoyl)anthranilic acid (ACA): a phospholipase A(2) inhibitor and TRP channel blocker. Cardiovasc Drug Rev. 2007;25(1):61-75. Epub 2007/04/21. doi: 10.1111/j.1527-3466.2007.00005.x. PubMed PMID: 17445088.
36. Moreno SN, Zhong L. Acidocalcisomes in Toxoplasma gondii tachyzoites. Biochem J. 1996;313 (Pt 2):655-9. PubMed PMID: 8573106.
37. Lovett JL, Marchesini N, Moreno SN, Sibley LD. Toxoplasma gondii microneme secretion involves intracellular Ca(2+) release from inositol 1,4,5-triphosphate (IP(3))/ryanodine-sensitive stores. J Biol Chem. 2002;277(29):25870-6. PubMed PMID: 12011085.
38. Lovett JL, Sibley LD. Intracellular calcium stores in Toxoplasma gondii govern invasion of host cells. J Cell Sci. 2003;116(Pt 14):3009-16. PubMed PMID: 12783987.
39. Bezzerides VJ, Ramsey IS, Kotecha S, Greka A, Clapham DE. Rapid vesicular translocation and insertion of TRP channels. Nat Cell Biol. 2004;6(8):709-20. Epub 2004/07/20. doi: 10.1038/ncb1150. PubMed PMID: 15258588.
40. Cai Y, Maeda Y, Cedzich A, Torres VE, Wu G, Hayashi T, et al. Identification and characterization of polycystin-2, the PKD2 gene product. J Biol Chem. 1999;274(40):28557-65. Epub 1999/09/25. doi: 10.1074/jbc.274.40.28557. PubMed PMID: 10497221.
41. Nagamune K, Beatty WL, Sibley LD. Artemisinin induces calcium-dependent protein secretion in the protozoan parasite Toxoplasma gondii. Eukaryotic cell. 2007;6(11):2147-56. Epub 2007/09/04. doi: 10.1128/EC.00262-07. PubMed PMID: 17766463; PubMed Central PMCID: PMC2168421.
42. Sagara Y, Inesi G. Inhibition of the sarcoplasmic reticulum Ca2+ transport ATPase by thapsigargin at subnanomolar concentrations. J Biol Chem. 1991;266(21):13503-6. Epub 1991/07/25. PubMed PMID: 1830305.
43. Thastrup O, Cullen PJ, Drobak BK, Hanley MR, Dawson AP. Thapsigargin, a tumor promoter, discharges intracellular Ca2+ stores by specific inhibition of the endoplasmic reticulum Ca2(+)-ATPase. Proc Natl Acad Sci U S A. 1990;87(7):2466-70. Epub 1990/04/01. PubMed PMID: 2138778; PubMed Central PMCID: PMCPMC53710.
44. Guerrero-Hernandez A, Dagnino-Acosta A, Verkhratsky A. An intelligent sarco-endoplasmic reticulum Ca2+ store: release and leak channels have differential access to a concealed Ca2+ pool. Cell Calcium. 2010;48(2-3):143-9. Epub 2010/09/08. doi: 10.1016/j.ceca.2010.08.001. PubMed PMID: 20817294.

45. Carreras-Sureda A, Pihan P, Hetz C. Calcium signaling at the endoplasmic reticulum: fine-tuning stress responses. Cell Calcium. 2018;70:24-31. Epub 2017/10/22. doi: 10.1016/j.ceca.2017.08.004. PubMed PMID: 29054537.
46. Miranda K, Pace DA, Cintron R, Rodrigues JC, Fang J, Smith A, et al. Characterization of a novel organelle in Toxoplasma gondii with similar composition and function to the plant vacuole. Molecular microbiology. 2010;76(6):1358-75. Epub 2010/04/20. doi: 10.1111/j.1365-2958.2010.07165.x. PubMed PMID: 20398214; PubMed Central PMCID: PMC2907454.
47. Ta CM, Vien TN, Ng LCT, DeCaen PG. Structure and function of polycystin channels in primary cilia. Cell Signal. 2020;72:109626. Epub 2020/04/07. doi: 10.1016/j.cellsig.2020.109626. PubMed PMID: 32251715; PubMed Central PMCID: PMCPMC7373203.
48. Kleene SJ, Kleene NK. The native TRPP2-dependent channel of murine renal primary cilia. Am J Physiol Renal Physiol. 2017;312(1):F96-F108. Epub 2016/10/21. doi: 10.1152/ajprenal.00272.2016. PubMed PMID: 27760766; PubMed Central PMCID: PMCPMC5283891.
49. Liu X, Vien T, Duan J, Sheu SH, DeCaen PG, Clapham DE. Polycystin-2 is an essential ion channel subunit in the primary cilium of the renal collecting duct epithelium. Elife. 2018;7. Epub 2018/02/15. doi: 10.7554/eLife.33183. PubMed PMID: 29443690; PubMed Central PMCID: PMCPMC5812715.
50. Vien TN, Wang J, Ng LCT, Cao E, DeCaen PG. Molecular dysregulation of ciliary polycystin-2 channels caused by variants in the TOP domain. Proc Natl Acad Sci U S A. 2020;117(19):10329-38. Epub 2020/04/26. doi: 10.1073/pnas.1920777117. PubMed PMID: 32332171; PubMed Central PMCID: PMCPMC7229662.
51. Kuo IY, Keeler C, Corbin R, Celic A, Petri ET, Hodsdon ME, et al. The number and location of EF hand motifs dictates the calcium dependence of polycystin-2 function. FASEB J. 2014;28(5):2332-46. Epub 2014/02/22. doi: 10.1096/fj.13-247106. PubMed PMID: 24558196; PubMed Central PMCID: PMCPMC3986840.
52. Yang Y, Keeler C, Kuo IY, Lolis EJ, Ehrlich BE, Hodsdon ME. Oligomerization of the polycystin-2 C-terminal tail and effects on its Ca2+-binding properties. J Biol Chem. 2015;290(16):10544-54. Epub 2015/02/27. doi: 10.1074/jbc.M115.641803. PubMed PMID: 25716316; PubMed Central PMCID: PMCPMC4400361.
53. DeCaen PG, Liu X, Abiria S, Clapham DE. Atypical calcium regulation of the PKD2-L1 polycystin ion channel. Elife. 2016;5. Epub 2016/06/28. doi: 10.7554/eLife.13413. PubMed PMID: 27348301; PubMed Central PMCID: PMCPMC4922860.
54. Chen XZ, Vassilev PM, Basora N, Peng JB, Nomura H, Segal Y, et al. Polycystin-L is a calcium-regulated cation channel permeable to calcium ions. Nature. 1999;401(6751):383-6. Epub 1999/10/12. doi: 10.1038/43907. PubMed PMID: 10517637.
55. Burgoyne T, Patel S, Eden ER. Calcium signaling at ER membrane contact sites. Biochim Biophys Acta. 2015;1853(9):2012-7. Epub 2015/02/11. doi: 10.1016/j.bbamcr.2015.01.022. PubMed PMID: 25662816.
56. Berridge MJ. Calcium microdomains: organization and function. Cell Calcium. 2006;40(5-6):405-12. Epub 2006/10/13. doi: 10.1016/j.ceca.2006.09.002. PubMed PMID: 17030366.
57. Mulier M, Vriens J, Voets T. TRP channel pores and local calcium signals. Cell Calcium. 2017;66:19-24. Epub 2017/08/16. doi: 10.1016/j.ceca.2017.04.007. PubMed PMID: 28807146.
58. Liu X, Ong HL, Ambudkar I. TRP Channel Involvement in Salivary Glands-Some Good, Some Bad. Cells. 2018;7(7). Epub 2018/07/13. doi: 10.3390/cells7070074. PubMed PMID: 29997338; PubMed Central PMCID: PMCPMC6070825.
59. Farwell DG, Shera KA, Koop JI, Bonnet GA, Matthews CP, Reuther GW, et al. Genetic and epigenetic changes in human epithelial cells immortalized by telomerase. Am J Pathol. 2000;156(5):1537-47. Epub 2000/05/04. doi: 10.1016/S0002-9440(10)65025-0. PubMed PMID: 10793065; PubMed Central PMCID: PMCPMC1876907.

60. Meissner M, Brecht S, Bujard H, Soldati D. Modulation of myosin A expression by a newly established tetracycline repressor-based inducible system in Toxoplasma gondii. Nucleic Acids Res. 2001;29(22):E115. Epub 2001/11/20. doi: 10.1093/nar/29.22.e115. PubMed PMID: 11713335; PubMed Central PMCID: PMCPMC92585.
61. Fox BA, Ristuccia JG, Gigley JP, Bzik DJ. Efficient gene replacements in Toxoplasma gondii strains deficient for nonhomologous end joining. Eukaryot Cell. 2009;8(4):520-9. Epub 2009/02/17. doi: 10.1128/EC.00357-08. PubMed PMID: 19218423; PubMed Central PMCID: PMCPMC2669201.
62. Shen B, Brown K, Long S, Sibley LD. Development of CRISPR/Cas9 for Efficient Genome Editing in Toxoplasma gondii. Methods Mol Biol. 2017;1498:79-103. Epub 2016/10/07. doi: 10.1007/978-1-4939-6472-7_6. PubMed PMID: 27709570.
63. Livak KJ, Flood SJ, Marmaro J, Giusti W, Deetz K. Oligonucleotides with fluorescent dyes at opposite ends provide a quenched probe system useful for detecting PCR product and nucleic acid hybridization. PCR Methods Appl. 1995;4(6):357-62. Epub 1995/06/01. doi: 10.1101/gr.4.6.357. PubMed PMID: 7580930.
64. Chasen NM, Asady B, Lemgruber L, Vommaro RC, Kissinger JC, Coppens I, et al. A Glycosylphosphatidylinositol-Anchored Carbonic Anhydrase-Related Protein of Toxoplasma gondii Is Important for Rhoptry Biogenesis and Virulence. mSphere. 2017;2(3). Epub 2017/05/23. doi: 10.1128/mSphere.00027-17. PubMed PMID: 28529974; PubMed Central PMCID: PMCPMC5437132.
65. Chasen NM, Stasic AJ, Asady B, Coppens I, Moreno SNJ. The Vacuolar Zinc Transporter TgZnT Protects Toxoplasma gondii from Zinc Toxicity. mSphere. 2019;4(3). Epub 2019/05/24. doi: 10.1128/mSphere.00086-19. PubMed PMID: 31118298; PubMed Central PMCID: PMCPMC6531880.
66. Laemmli UK. Cleavage of structural proteins during the assembly of the head of bacteriophage T4. Nature. 1970;227(5259):680-5. Epub 1970/08/15. doi: 10.1038/227680a0. PubMed PMID: 5432063.
67. Liu J, Pace D, Dou Z, King TP, Guidot D, Li ZH, et al. A vacuolar-H(+) -pyrophosphatase (TgVP1) is required for microneme secretion, host cell invasion, and extracellular survival of Toxoplasma gondii. Mol Microbiol. 2014;93(4):698-712. Epub 2014/07/01. doi: 10.1111/mmi.12685. PubMed PMID: 24975633; PubMed Central PMCID: PMCPMC4159726.
68. Schindelin J, Arganda-Carreras I, Frise E, Kaynig V, Longair M, Pietzsch T, et al. Fiji: an open-source platform for biological-image analysis. Nat Methods. 2012;9(7):676-82. Epub 2012/06/30. doi: 10.1038/nmeth.2019. PubMed PMID: 22743772; PubMed Central PMCID: PMCPMC3855844.
69. Grynkiewicz G, Poenie M, Tsien RY. A new generation of Ca2+ indicators with greatly improved fluorescence properties. J Biol Chem. 1985;260(6):3440-50. PubMed PMID: 3838314.
70. Alzayady KJ, Wagner LE, 2nd, Chandrasekhar R, Monteagudo A, Godiska R, Tall GG, et al. Functional inositol 1,4,5-trisphosphate receptors assembled from concatenated homo- and heteromeric subunits. J Biol Chem. 2013;288(41):29772-84. Epub 2013/08/21. doi: 10.1074/jbc.M113.502203. PubMed PMID: 23955339; PubMed Central PMCID: PMCPMC3795275.
71. Longo PA, Kavran JM, Kim MS, Leahy DJ. Transient mammalian cell transfection with polyethylenimine (PEI). Methods Enzymol. 2013;529:227-40. Epub 2013/09/10. doi: 10.1016/B978-0-12-418687-3.00018-5. PubMed PMID: 24011049; PubMed Central PMCID: PMCPMC4012321.
72. Mak DO, Vais H, Cheung KH, Foskett JK. Nuclear patch-clamp electrophysiology of Ca2+ channels. Cold Spring Harb Protoc. 2013;2013(9):885-91. Epub 2013/09/05. doi: 10.1101/pdb.prot073064. PubMed PMID: 24003194; PubMed Central PMCID: PMCPMC3984033.
73. Henderson MJ, Baldwin HA, Werley CA, Boccardo S, Whitaker LR, Yan X, et al. A Low Affinity GCaMP3 Variant (GCaMPer) for Imaging the Endoplasmic Reticulum Calcium Store. PLoS One. 2015;10(10):e0139273. Epub 2015/10/10. doi: 10.1371/journal.pone.0139273. PubMed PMID: 26451944; PubMed Central PMCID: PMCPMC4599735.

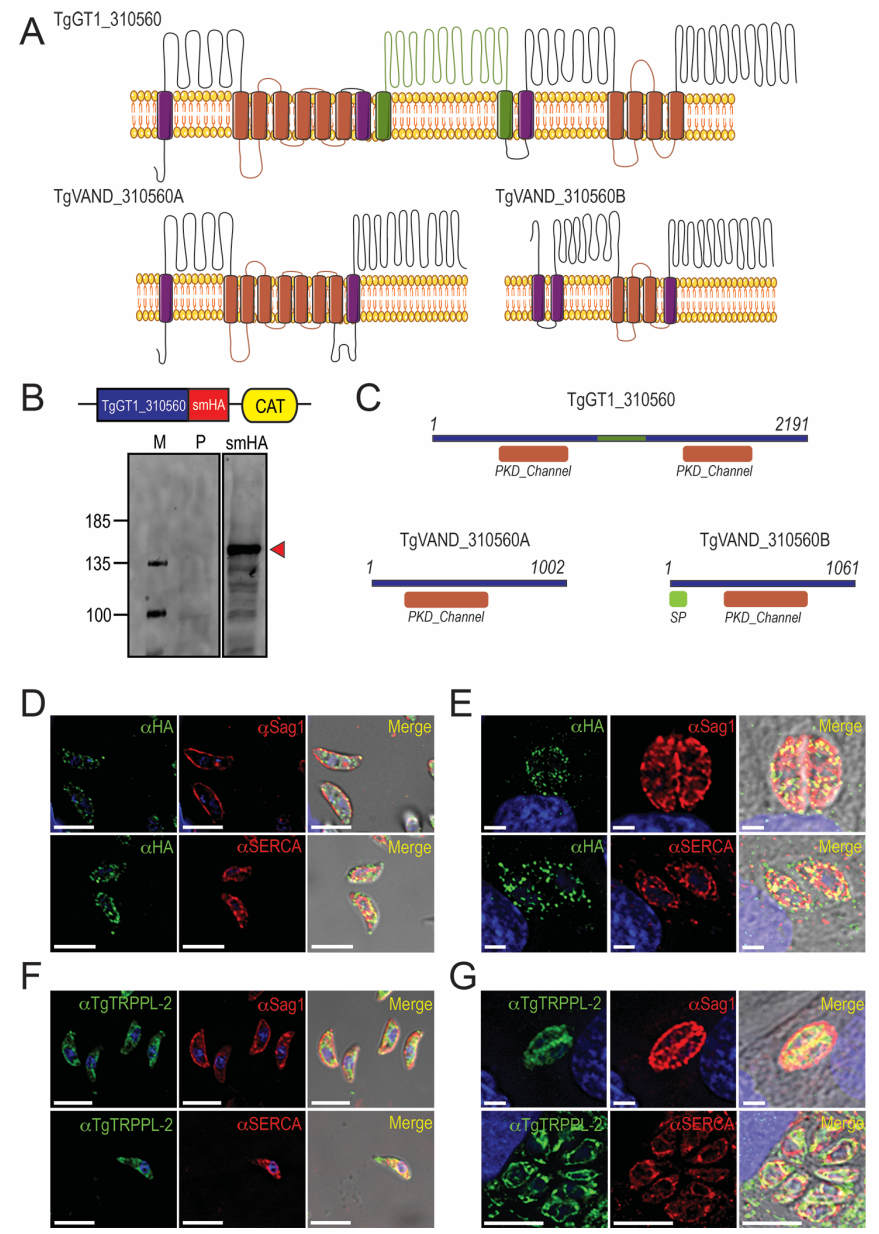

Figure 1. TgTRPPL-2 localizes to the plasma membrane (PM) and ER of *T. gondii*. A. Predicted topology for TgTRPPL-2 in GT1 and VAND strains. Model was generated with the Protter application [21]. The PKD Domain is highlighted in orange. The domain used to generate antibodies is highlighted in green. **B.** Schematic representation of C-terminal tagging of TgTRPPL-2 in TatiΔKu80 parasites and western blots of TgTRPPL-2-smHA membranes using αHA (1:1,000) showing a major band at approximately 150 kDa (*red arrowhead*). **C.** Schematic representation of the InterPro Domain annotation of TgTRPPL-2 in GT1 and VAND strains. **D.** IFAs of extracellular tachyzoites using αHA antibody show vesicular staining close to the PM and intracellular. Co-localization with αSAG1 and αSERCA show partial co-localization with both markers. **E.** IFAs of intracellular tachyzoites with αHA (1:100), αSag1 (1:1,000) and αSERCA (1:1,000) showing co-localization at the PM and ER. **F-G.** IFAs of extracellular and intracellular tachyzoites respectively with αTRPPL-2 (1:1,000) showing labeling of the protein at the periphery, co-localized with αSAG1 (1:1,000) and ER co-localized with αTgSERCA (1:1,000).

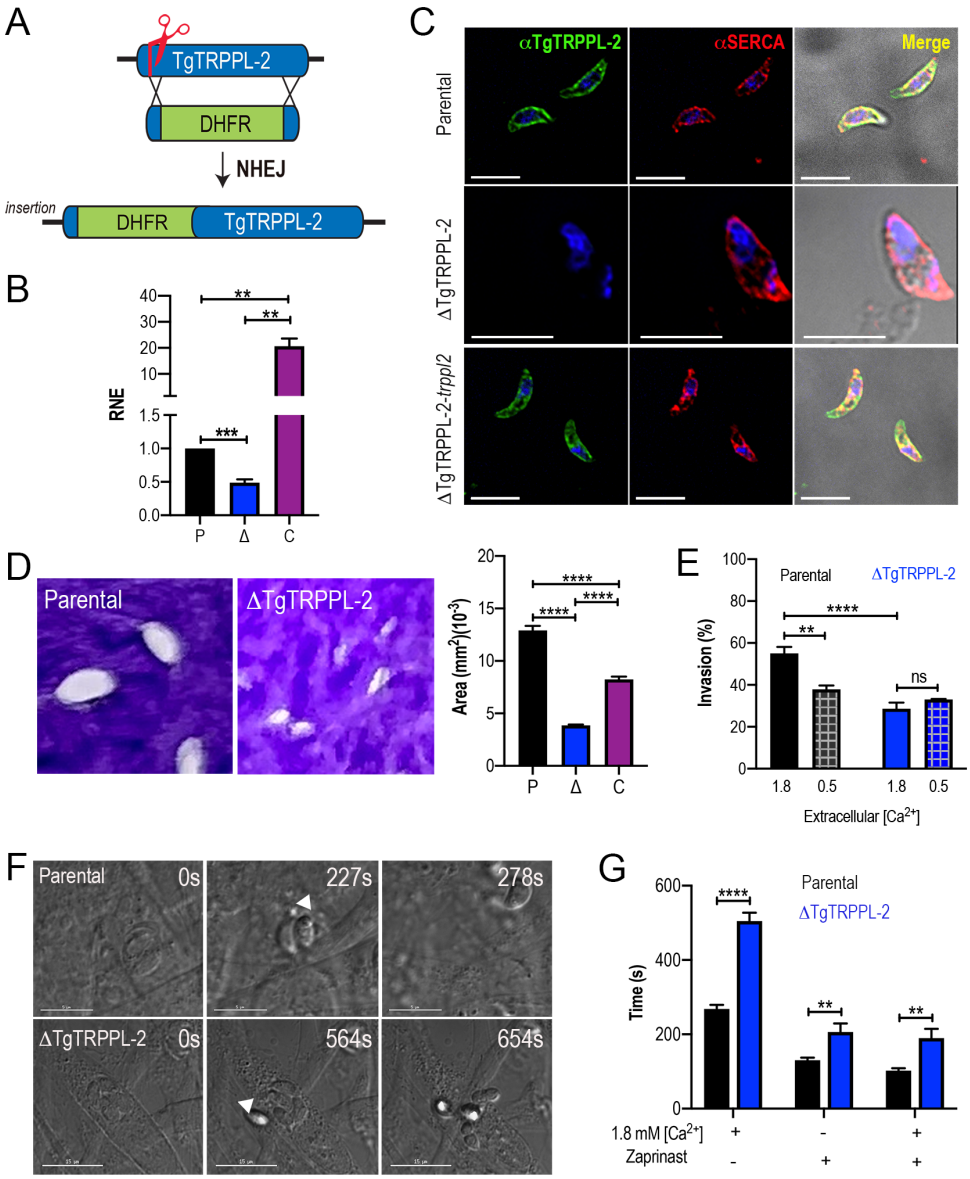

Figure 2. TgTRPPL-2 and its role in *T. gondii* growth. Schematic representation of the generation of *ΔTgTRPPL-2* in the *T. gondii* RH strain. **B.** qPCR of total RNA from *ΔTgTRPPL-2*, *ΔTgTRPPL-2-trppl2* and parental strains using primers upstream and downstream of the insertion site of the DHFR cassette. **C.** IFAs of extracellular parasites showing PM labeling with αTgTRPPL2 (1:1,000) and co-localization with αSERCA (1:1,000). **D**. Plaque assays of parental (P), *ΔTgTRPPL-2* (Δ) and *ΔTgTRPPL-2-trppl2* (C) cells. Quantification of plaque sizes from three independent biological experiments using student's t-test. ****p< 0.0001. **E.** Red green assays of parental, *ΔTgTRPPL-2* and *ΔTgTRPPL-2-trppl2* cells quantifying invaded and attached intracellular parasites. Assays were done at two concentrations of extracellular Ca^{2+}: 0.5 and 1.8 mM. Asterisk indicate p value for significant difference, ** p< 0.001, **** p< 0.0001. **F.** Time to egress stimulated by saponin/Ca^{2+} at 1.8 mM extracellular Ca^{2+} of both parental or *ΔTgTRPPL-2 mutants*. **G.** Statistical analysis of average time to egress stimulated by saponin/Ca^{2+} or Zaprinast in the presence or absence of extracellular calcium. Analysis was performed from three independent biological replicates using student's t-test. Asterisk indicate p value for significant difference. ** p< 0.003, **** p<0.0001. *Black bars* represent parental strain, *blue bars* represent ΔTgTRPPL-2.

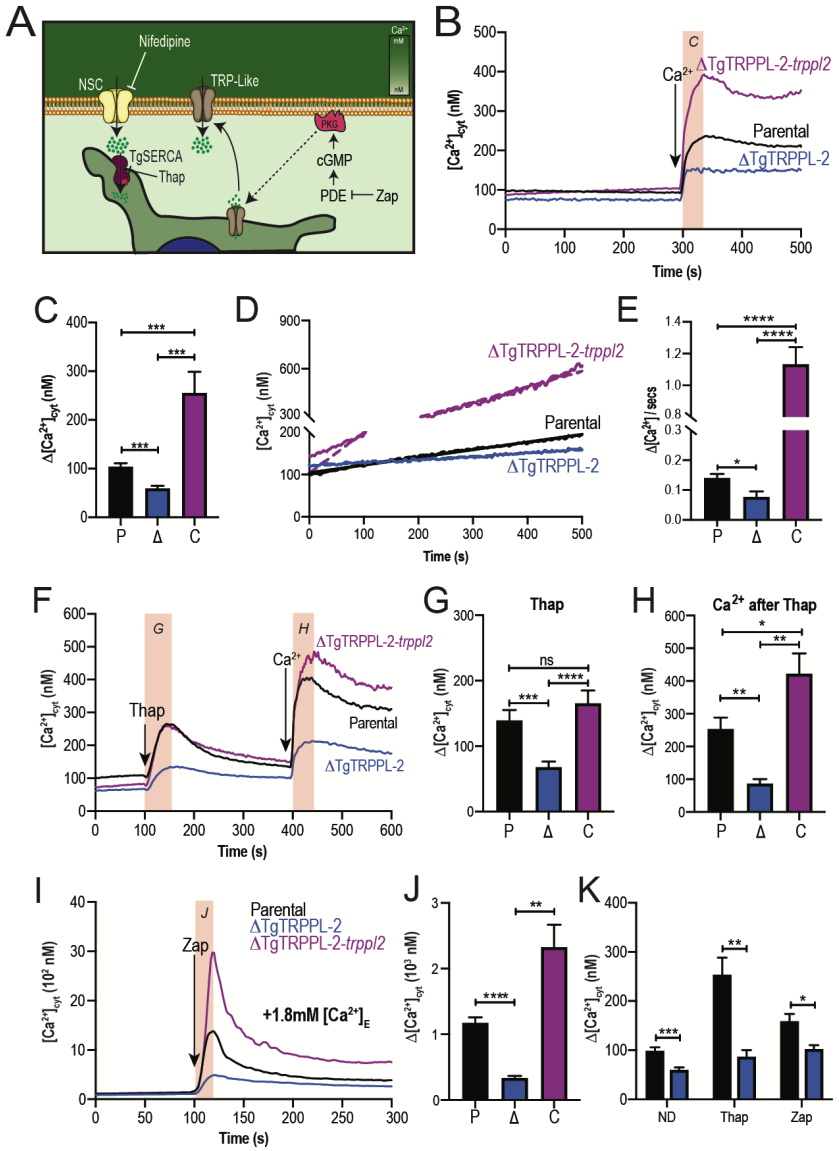

Figure 3. The role of TgTRPPL-2 in PM Ca^{2+} influx. A. Scheme showing the mechanism of Ca^{2+} influx and how cytosolic Ca^{2+} may activate the PM channel (Ca^{2+}-activated Calcium Entry). *NSC, Nifedipine-Sensitive Channel; PKG, Protein Kinase G; PDE, phosphodiesterase; Thap, Thapsigargin*. **B.** Cytosolic Ca^{2+} measurements of Fura-2 loaded tachyzoites of the parental (P), *ΔTgTRPPL-2* (Δ) and *ΔTgTRPPL-2-trppl2* (C) lines. The buffer contains 100 µM EGTA and 1.8 mM Ca^{2+} was added at 300 sec. The *orange box* indicated the area used for the quantification presented in *C*. **C.** Quantification and statistical analysis of the change in cytosolic Ca^{2+} during the first 20 s after addition of extracellular Ca^{2+}. *** p< 0.0002. **D.** Cytosolic Ca^{2+} increase of parasites pre-incubated with 1.8 mM Ca^{2+}. **E.** Quantification and statistical analysis of the slope from *D*. **** p< 0.0001. **F.** Ca^{2+} efflux after adding Thap (1 μM) followed by Ca^{2+} influx after the addition of 1.8 mM extracellular Ca^{2+}. *Orange box* indicates the area used for the quantification presented in *G* and *H*. **G.** Quantification and statistical analysis of the change in cytosolic Ca^{2+} 50 s after the addition of Thap *(Thap)*. **H,** similar quantification to the one in G, 20 s after the addition of 1.8 mM of Ca^{2+} *(Ca^{2+} after Thap)*. *** p< 0.0008, **** p<0.0001. **G.** Calcium-activated Calcium Entry with Zaprinast (100 μM) in the presence of 1.8 mM extracellular Ca^{2+}. **J.** Quantification and statistical analysis of cytosolic Ca^{2+} increase during the first 15 s after adding Zaprinast (100 μM) (*Orange box*, in I). ** p< 0.001, **** p< 0.0001. **K.** Quantification and statistical analysis of Ca^{2+} influx during the 20 s after adding Ca^{2+} without additions (ND) or after adding Thap or Zap. * p< 0.02, ** p< 0.005, *** p< 0.0008. Statistical analysis for all experiments were done from at least three independent trials using student's t-test. P values are indicated with asterisks for each panel.

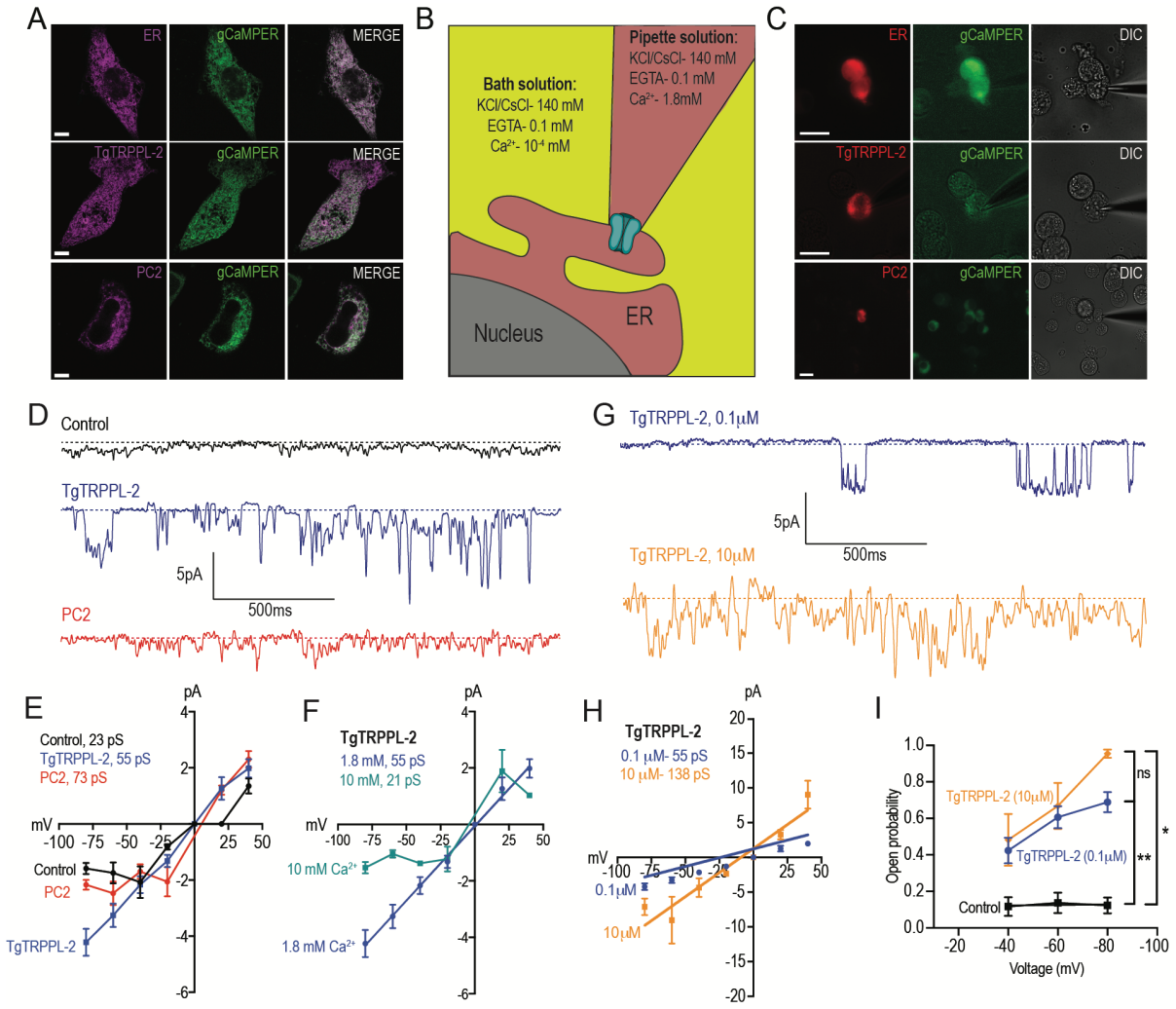

Figure 4. Functional studies of TgTRPPL-2 expressed in HEK-3KO cells. A, Images of 3KO-HEK cells expressing an ER-marker, PC2 or TgTRPPL-2 with the genetic calcium indicator gCAMPER. **B.** Schematic representation of nuclear-ER patch clamp arrangements. Ionic composition and concentration for bath and pipette solutions are shown. **C.** Patched nuclear-extract expressing ER-marker, PC2 or TgTRPPL-2 with the genetic calcium indicator gCaMPER. **D.** Representative tracing of currents recorded in the presence of 1.8 mM luminal Ca^{2+} in 140 mM KCl solution of Control, *TgTRPPL-2* or *PC2* expressing cells. Tracings represent ~2 s from 25 s recording and filtered at 45 kHz. **E.** Current-voltage relationship comparing single-channel conductance shown in *D* of Control, PC2 and TgTRPPL-2 expressing cells. *Inset*, calculated channel conductance for control, TgTRPPL-2 and PC2 from -80 to -40 mVs. **F.** Current-voltage relationship comparing single-channel conductance of TgTRPPL-2 expressing cells at 1.8 and 10 mM [Ca^{2+}] in the pipette solution. *Inset*, calculated channel conductance for the conditions analyzed. **G.** Representative tracing of currents recorded from TgTRPPL-2 expressing cells using different concentration of [Ca^{2+}] in the bath solution (Solution A vs. Solution B) (Table S4). Tracings represent ~2 s from a 25 s recording and filtered at 45 kHz. **H.** Current-voltage relationship comparing single-channel conductance of TgTRPPL-2 expressing cells at 0.1 and 10 μM [Ca^{2+}] in the bath solution. *Inset*, calculated channel conductance for the different [Ca^{2+}]. **I.** Open probability of control and TgTRPPL-2 expressing cells in the presence of different [Ca^{2+}] in the bath solution in comparison to the Control. Asterisk indicate p value for significant difference. *p< 0.01, **p<0.001.

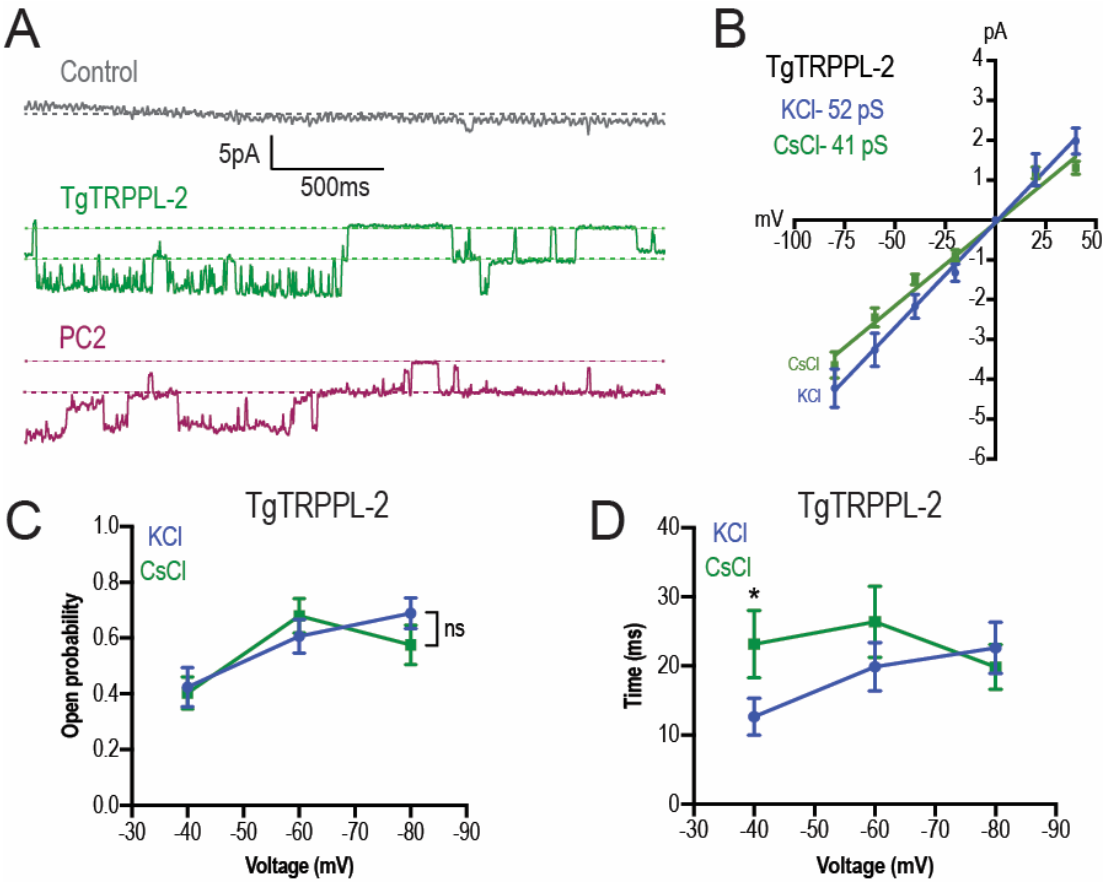

Figure 5. TgTRPPL-2 permeates Ca^{2+}. A. Representative tracing of currents recorded at -80 mV in the presence of 1.8 mM Ca^{2+} inside the pipette (Solution D, Table S4) of nuclear extracts from Control, *TgTRPPL-2* or *PC2* expressing cells. Traces are a representation of 2 seconds of sampling from a total time of 25 seconds. **B.** Current-voltage relationship comparing single-channel conductance of TgTRPPL-2 cells in 1.8 mM Ca^{2+} in KCl (*blue*) or CsCl (*green*) buffer. *Inset*, Channel conductance of TgTRPPL-2 in the different conditions analyzed. **C.** Calculated open probability of TgTRPPL-2 expressing cells in the presence of 1.8 mM Ca^{2+} in a KCl (*blue*) or CsCl (*green*) buffer. **D.** Average time of channel opening of TgTRPPL-2 expressing cells in the presence of 1.8 mM Ca^{2+} in a KCl (*blue*) or CsCl (*green*). Asterisk indicate p value for significant difference. * $p< 0.04$.

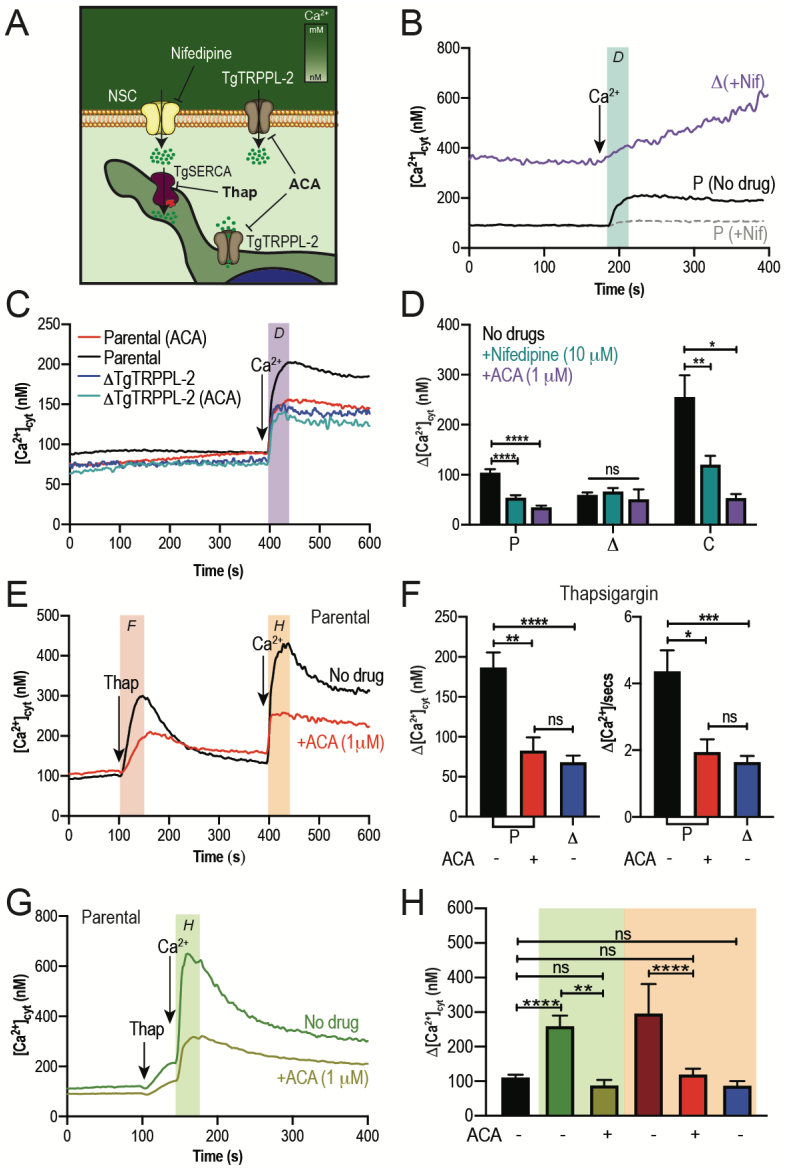

Figure 6. Regulation of TgTRPPL-2 by Ca^{2+} and inhibition by TRP inhibitors. A. Scheme showing TgTRPPL-2 acting at the PM and ER. **B**. Cytosolic Ca^{2+} measurements of Fura2 loaded tachyzoites pre-incubated with 10 μM nifedipine. 1.8 mM Ca^{2+} was added where indicated. The *blue box* indicates the area used for the quantification presented in *D*. **C.** Cytosolic Ca^{2+} measurements of suspensions of parental and *ΔTgTRPPL-2* parasites pre-incubated for 3 min with ACA (1 μM). 1.8 mM Ca^{2+} was added where indicated. *Purple box* shows the area used for the quantifications presented in *D*. **D.** Change in cytosolic Ca^{2+} during the first 20 s after addition of Ca^{2+} in the presence of 10 μM of nifedipine or 1 μM ACA. Asterisk indicate p value for significant difference. * p<0.01, ** p<0.003, **** p<0.0001. **E.** Cytosolic Ca^{2+} increase after adding Thap (1 μM) to a suspension of tachyzoites. The red line shows a similar experiment but the cells were pre-incubated with ACA for 3 min. *Pink and orange boxes* show the areas used for the quantifications presented in *F*. **F.** Quantification and statistical analysis of the ΔCa^{2+} and slope 50 s after the addition of Thap in the presence or absence of ACA in parental and *ΔTgTRPPL-2* mutants. Asterisk indicate p value for significant difference, *p< 0.01, **p< 0.003 ***p< 0.0003. **G.** Stimulation of Ca^{2+} influx by pre-addition of Thap in the presence or absence of 1 μM ACA. Green box shows the area used for the quantifications presented in H. **H.** Quantification of change of cytosolic Ca^{2+} 20 s after the addition of 1.8 mM Ca^{2+} following the addition of Thap under different conditions. Asterisk indicate p value for significant difference. **p<0.001, ****p<0.00001. The statistical analysis for all experiments were done from at least three independent trials using student's t-test.

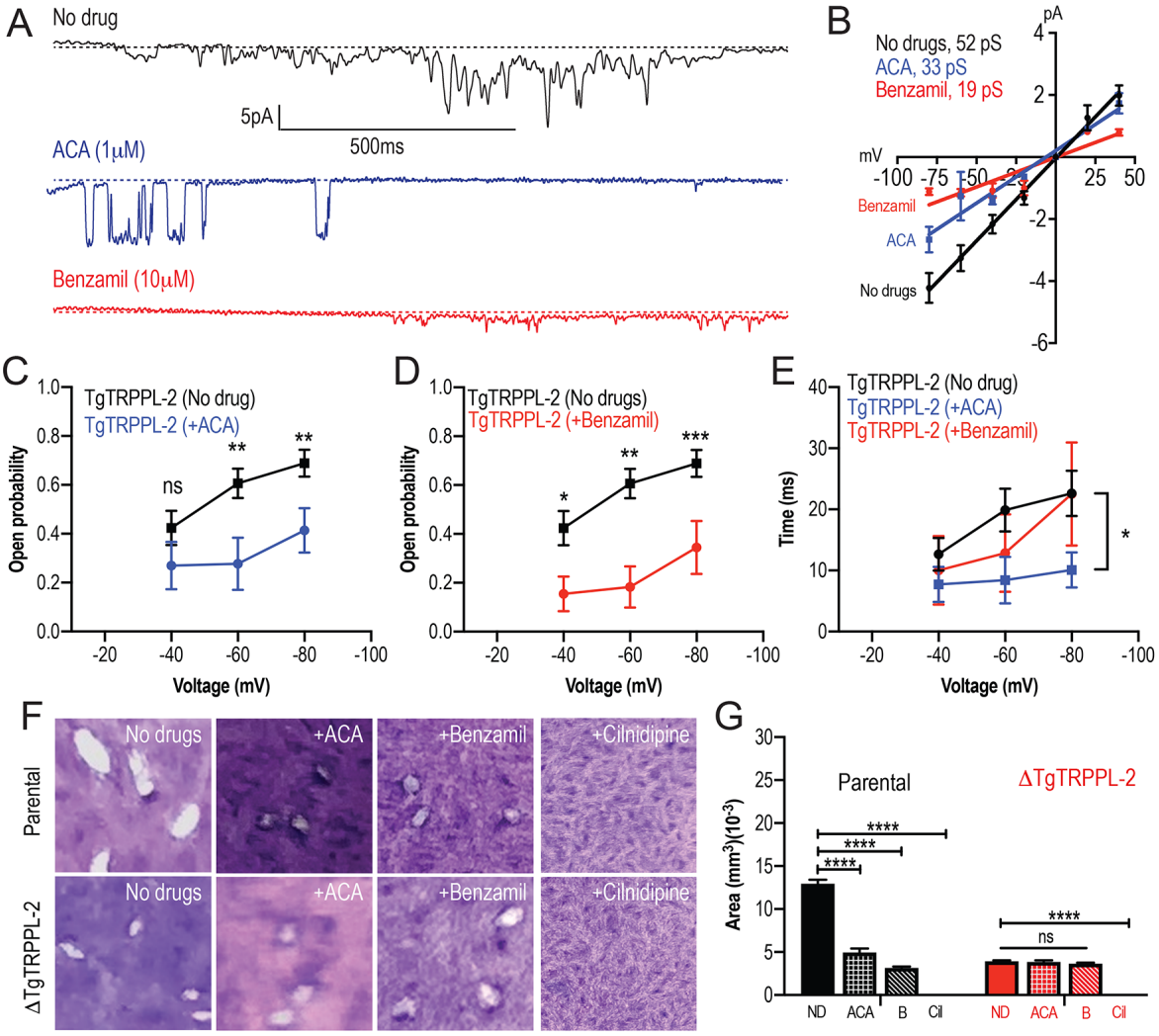

Figure 7. TRP Inhibitors decreased the activity of TgTRPPL-2. A. Example of currents recorded of *TgTRPPL-2* expressing cells at –80 mV without drug (*Black trace*) versus in the presence of 1 μM of ACA (*Blue trace*) or 10 μM of benzamil (*Red trace*). **B.** Current-voltage relationship comparing single-channel conductance in the presence of ACA or benzamil. Analysis was done from three independent biological trials. *Inset*, conductance of TgTRPPL-2 in the different conditions analyzed. **C.** Calculated open probability of TgTRPPL-2 expressing cells (*black*) or in the presence of ACA (*blue*). Asterisk indicate p value for significant difference. ** p< 0.006-0.007. **D.** Calculated open probability of TgTRPPL-2 expressing cells (*black*) or in the presence of Benzamil (*red*). Asterisk indicate p value for significant difference. * p< 0.02, ** p< 0.002, *** p< 0.0002. **E.** Average time of channel opening of TgTRPPL-2 expressing cells in the presence of TRP inhibitors. Asterisk indicate p value for significant difference. * p< 0.02 **F.** Plaque assay of *ΔTgTRPPL-2* mutants and the parental strain in the presence of ACA (1 μM), benzamil (10 μM) (B) and cilnidipine (40 μM) (Cil) after 7 days of growth. ND means no drug. **G**. Quantification and statistical analysis of plaque sizes from three independent biological replicates using student's *t*-test. *ND, no drug, B, Benzamyl, Cil: Cilnedipine*. Asterisk indicate p value for significant difference. ****p< 0.0001.

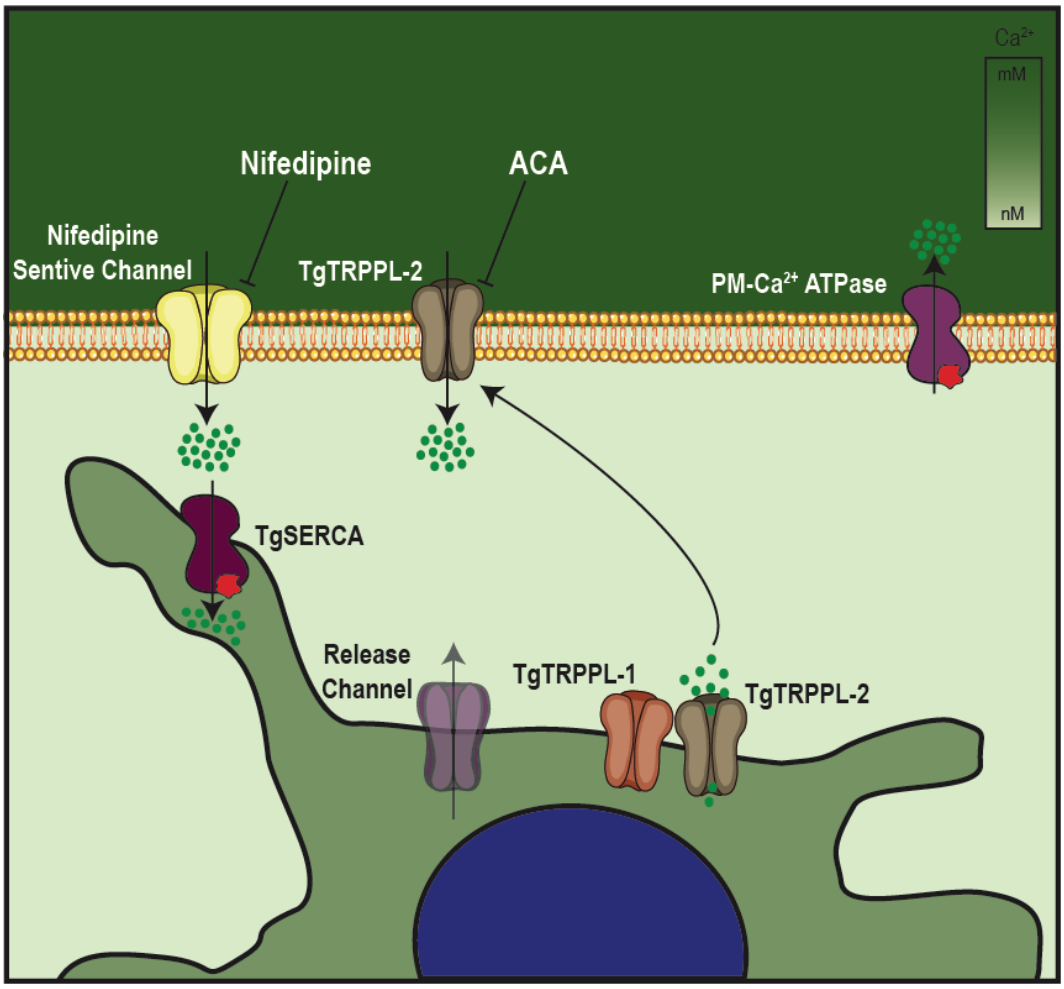

Figure 8. The role of TgTRPPL-2 in Ca^{2+} influx into the cytosol of *T. gondii*. Schematic representation of the Ca^{2+} influx pathways of *T. gondii*. Ca^{2+} influx may be mediated by two independent Ca^{2+} channels, a nifedipine-sensitive channel (still uncharacterized) and TgTRPPL-2 (the subject of this work). TgTRPPL-2 localizes to the plasma membrane as well as the ER. TgTRPPL-2 is a cation permeable channel that mediates Ca^{2+} influx by a pathway that is activated by high [Ca^{2+}] and can be inhibited by broad TRP inhibitors like ACA and benzamil. The presence of the channel at the ER suggest that it may function as a Ca^{2+} efflux channel. Increase in cytosolic [Ca^{2+}] can modulate TgTRPPL-2 by allowing the channel to open for longer time thus allowing more Ca^{2+} to enter the cell. We hypothesize the presence of a release channel at the ER membrane likely responsive to the second messenger IP_3 [38]. We also hypothesize a potential interaction between TgTRPPL-1 and TgTRPPL-2.

Calcium signaling by a Transient Receptor Channel is critical for *Toxoplasma gondii* growth

Márquez-Nogueras et al

Supplemental tables and Figures

Table S1: Top 10 hits of HHPRED analysis of TgTRPPL-2.

Name	Probability	E-value	AA lenght	PDB Reference
Polycystic kidney disease 2-like 1	99.45	7.10 E^{-11}	805	6DU8_A
Polycystin-2; PKD2	99.44	1.10 E^{-10}	756	6WB8_D
Polycystic kidney disease 2-like 1	99.39	2.10 E^{-10}	566	5Z1W_C
Polycystin-2, Polycystin-1	99.38	2.40 E^{-10}	577	6A70_A
Polycystin-2	99.35	2.40 E^{-10}	968	5MKE_A
Polycystin-2, Polycystin-1	99.3	2.80 E^{-10}	1153	6A70_B
Polycystin-2; TRP channel, PKD2	99.22	3.30 E^{-09}	510	5T4D_A
TRPV2; Transport protein, TRP channel	98.52	6.6 E^{-05}	613	5AN8_B
Mucolipin-3; TRP channel, lysosomal	98.31	0.00031	558	6AYF_C
Transient receptor potential cation channel	98.28	0.00015	639	6LGP_D

Table S2: List of Mass spectrometry hits by TgTRPPL-2 Immunoprecipitation*.

Gene ID	Description	Phenotype#	TMD	Average counts
TgGT1_310560	Hypothetical protein (TgTRPPL-2)	-2.49	13	3
TgGT1_247370	Hypothetical protein (TgTRPPL-1)	-1.42	13	3
TgGT1_214300	Hypothetical Protein	-0.36	9	3
TgGT1_280560	Selenide, water dikinase	0.07	0	6
TgGT1_201680	Putative eukaryotic initiation factor-3 subunit 10	-4.55	0	6
TgGT1_228170	Inner membrane complex protein IMC2A	-3.28	1	5.5
TgGT1_212300	Hypothetical protein	0.69	1	3
TgGT1_229180	HEAT repeat-containing protein	-5.05	0	3

*See Experimental Procedures for the protocol.

Fitness score for each gene was obtained from ToxoDB.

Table S3: Primers used in this work

Endogenous Tagging of TgTRPPL2		
T1	TgTRPPL2_pLic_F	TACTTCCAATCCAATTTAATGCGAGAAGCGCATT GAGGAATGG
T2	TgTRPPL2_pLic_F	TCCTCCACTTCCAATTTTAGCCTCTTCTCCCAGG ATGTTGACGC
T3	TgTRPPL2_Validation_Tag_F	TATGTGTGCCTGCCTGCGCAT
Disruption of TgTRPPL2		
K1	TgTRPPL2_Cas9_gRNA_F	TATGTCACATGTCTTTTCTCGTTTTAGAGCTAGAA ATAGCAAG
K2	TgTRPPL2_DHFR_F	CTTTGGTTTCCCTCTCTCGTCCATGAAGCTTCGCC AGGCTGTAAATCC
K3	TgTRPPL2_DHFR_R	TGGACGCCCAGCTCGACATGTCATCCTGCAAGTG CATAGAAGGA
K4	TgTRPPL2_Validation R	CGATGAGGTGGATGTAGCTGAATG
RT-PCR of TgTRPPL2		
Q1	TgTRPPL2_qPCR_F	GAGCTCCGACGCAGGCCAGCAG
Q2	TgTRPPL2_qPCR_R	CCCGGGCGATGAGGTGGATGTAGCTGAATG
Cloning for Heterologous expression in DT-40-3KO cells		
C1	pCDNA3_TgTRPPL2_F	cagatatccatcacactggcATGCATGCATTCGACGAC
C2	tdTomato_TgTRPPL2_R	tgctcaccatCTCTTCTCCCAGGATGTTG
C3	TgTRPPL2_tdTomato_F	gggagaagagATGGTGAGCAAGGGCGAG
C4	pCDNA3_TgTRPPL2_tdTomato _R	acactatagaatagggccctCTACTTGTACAGCTCGTCC ATG
C5	TgTRPPL2_Validation_F	GCAAGAAGAAGAAACGACGCAAG
C6	TgTRPPL2_Validation_R	CTTTGAGGTCCTAGTTCACCTCCGA

Table S4. Composition of the solutions used for the electrophysiological analysis.

Reagents	Concentration (mM)				
	Solution A	**Solution B**	**Solution C**	**Solution D**	**Solution E**
KCl	140	140	140	-	-
CsCl	-	-	-	140	140
EGTA	0.1	0.1	0.1	0.1	0.1
Intracellular Ca^{2+}	1.8	10	1.8	1.8	10
Extracellular Ca^{2+}	0.0001	0.0001	0.01	0.0001	0.0001

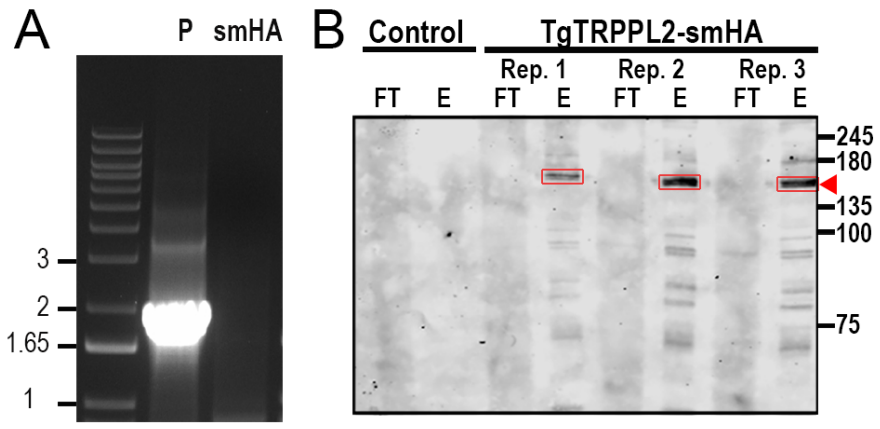

Figure S1. Validation of C-terminal tagging of TgTRPPL-2-smHA. A. Amplification of ~2 kB in the TgTRPPL-2-smHA cell line validating the correct integration of TgTRPPL-2-smHA. **B.** Western blot of three biological replicates of immunoprecipitated TgTRPPL-2-smHA using αHA antibody (1:1,000) shows a band of ~150kDa (highlighted by *red boxes* and *arrow*). No band is present in the control cell line.

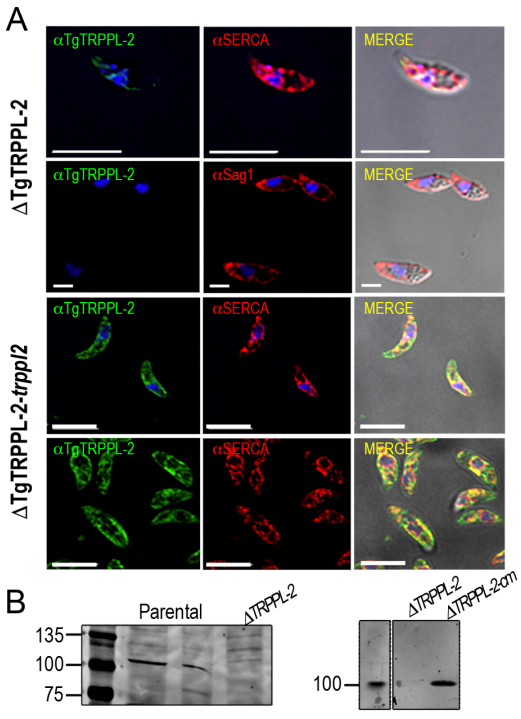

Figure S2. Validation of the anti-TgTRPPL-2 antibody. A, IFAs of extracellular tachyzoites with αTgTRPPL-2 (1:1,000) co-localized with αSERCA (1:1,000) in ΔTgTRPPL-2 and ΔTgTRPPL-2-*trppl2*. Images were taken with equivalent time and laser power. B, Western blots of lysates from parental, ΔTgTRPPL-2 and ΔTgTRPPL-2-*trppl2* cell were run in an SDS-PAGE cell and developed with anti-TgTRPPL-2 antibody at 1;1,000.

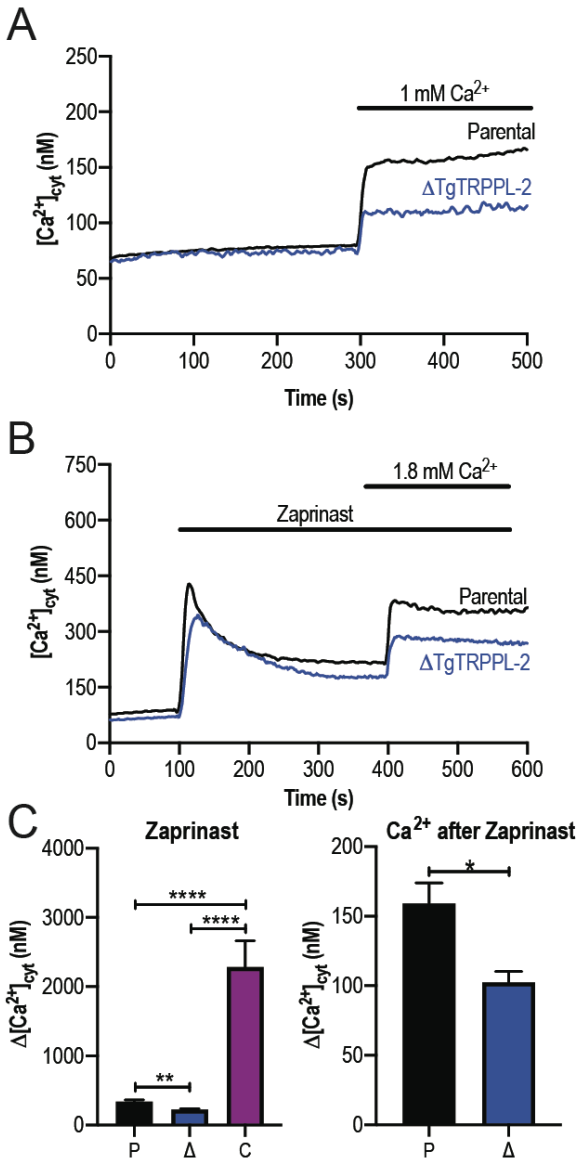

Figure S3. TgTRPPL-2 regulates Ca^{2+} in *T. gondii*. **A.** Cytosolic Ca^{2+} measurements of Fura-2 loaded tachyzoites of the parental and *ΔTgTRPPL-2* cell lines after addition of 1 mM extracellular Ca^{2+} at 300 s. **B.** Cytosolic Ca^{2+} measurement after the addition of Zaprinast (100 μM) at 100 s and Ca^{2+} influx was stimulated by the addition of 1.8 mM extracellular Ca^{2+} at 400s. **C.** Change in cytosolic Ca^{2+} 15 s after the addition of Zaprinast *(Labeled Zaprinast)* and 20 s after the addition of 1.8 mM of extracellular Ca^{2+} *(Labeled Ca^{2+} after Zaprinast)*. Asterisk indicate p value for significant difference. **p< 0.007, ****p< 0.0001.

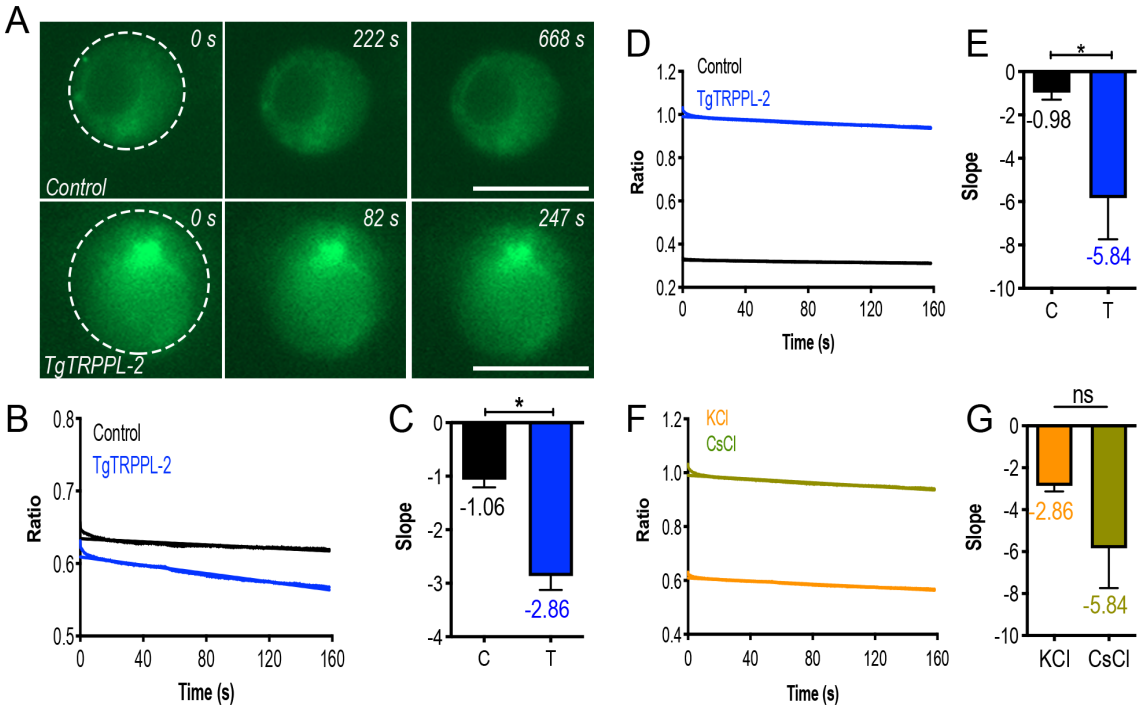

Figure S4. Measurement of ER Calcium of DT40-3KO cells expressing TgTRPPL-2. A. Fluorescence of ER calcium in ER-RFP-DT40 (*Control*) vs. TgTRPPL-2-DT40 (*TgTRPPL-2*) in a high calcium-potassium solution of patched nuclear membranes while the membrane is depolarized. **B.** Quantification of fluorescence of patched cells while the membrane is depolarized from -80 to +20 mV in a high calcium-potassium solution. **C.** Quantification of the slope of fluorescence in *B* comparing TgTRPPL-2-DT40-3KO cells versus the control cells. Slope of the fluorescence was quantified based on the 5 technical replicates of the artificial membrane depolarization in each cell analyzed. Asterisk indicate p value for significant difference. Values represent the mean of the slope shown in *B*. * p< 0.01. **D.** Quantification of fluorescence of patched cells while the membrane is depolarized from -80 to +20 mV in a High calcium-cesium solution. **E.** Quantification of the slope of fluorescence in *D* comparing TgTRPPL-2-DT40-3KO cells versus control cells. The slope was quantified for the five technical replicates of patched membranes. Asterisk indicate p value for significant difference. Values represent the mean of the slope shown in *D*. * p< 0.03. **F.** Comparison of the fluorescence of patched nuclear extract of TgTRPPL-2-DT40 cells while the membrane was artificially depolarized. **G.** Quantification of the slope of fluorescence of patched TgTRPPL-2-DT40-3KO nuclear extracts in different experimental conditions. Slope of the fluorescence was quantified based on the 5 technical replicates of the artificial membrane depolarization in each cell analyzed.